

ISS Debris Avoidance Maneuver Threshold Analysis

*J. L. Foster, Jr., Ph. D.
Barrios Technology, Ltd.*

*M. B. Wortham
J. H. Frisbee, Jr.
United Space Alliance, LLC*

This document was originally written in October of 1999.

THE NASA STI PROGRAM OFFICE . . . IN PROFILE

Since its founding, NASA has been dedicated to the advancement of aeronautics and space science. The NASA Scientific and Technical Information (STI) Program Office plays a key part in helping NASA maintain this important role.

The NASA STI Program Office is operated by Langley Research Center, the lead center for NASA's scientific and technical information. The NASA STI Program Office provides access to the NASA STI Database, the largest collection of aeronautical and space science STI in the world. The Program Office is also NASA's institutional mechanism for disseminating the results of its research and development activities. These results are published by NASA in the NASA STI Report Series, which includes the following report types:

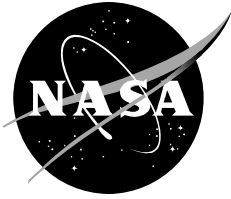
- **TECHNICAL PUBLICATION.** Reports of completed research or a major significant phase of research that present the results of NASA programs and include extensive data or theoretical analysis. Includes compilations of significant scientific and technical data and information deemed to be of continuing reference value. NASA's counterpart of peer-reviewed formal professional papers but has less stringent limitations on manuscript length and extent of graphic presentations.
- **TECHNICAL MEMORANDUM.** Scientific and technical findings that are preliminary or of specialized interest, e.g., quick release reports, working papers, and bibliographies that contain minimal annotation. Does not contain extensive analysis.
- **CONTRACTOR REPORT.** Scientific and technical findings by NASA-sponsored contractors and grantees.
- **CONFERENCE PUBLICATION.** Collected papers from scientific and technical conferences, symposia, seminars, or other meetings sponsored or cosponsored by NASA.
- **SPECIAL PUBLICATION.** Scientific, technical, or historical information from NASA programs, projects, and mission, often concerned with subjects having substantial public interest.
- **TECHNICAL TRANSLATION.** English-language translations of foreign scientific and technical material pertinent to NASA's mission.

Specialized services that complement the STI Program Office's diverse offerings include creating custom thesauri, building customized databases, organizing and publishing research results . . . even providing videos.

For more information about the NASA STI Program Office, see the following:

- Access the NASA STI Program Home Page at <http://www.sti.nasa.gov>
- E-mail your question via the internet to help@sti.nasa.gov
- Fax your question to the NASA Access Help Desk at (301) 621-0134
- Telephone the NASA Access Help Desk at (301) 621-0390
- Write to:
NASA Access Help Desk
NASA Center for Aerospace Information
7121 Standard
Hanover, MD 21076-1320

NASA/ TP-2007-214752



ISS Debris Avoidance Maneuver Threshold Analysis

J. L. Foster, Jr., Ph. D.
Barrios Technology, Ltd.

M. B. Wortham
J. H. Frisbee, Jr.
United Space Alliance, LLC

This document was originally written in January of 1999.

National Aeronautics and
Space Administration

Lyndon B. Johnson Space Center
Houston, Texas 77058

May 2007

Acknowledgement

The authors would like to acknowledge contributions to this paper of Brenda Moulton (JSC/DM), the NASA Project Lead. Jon Weaver (JSC/DM) was always available for discussion, and Herb Estes (JSC/EG) made a considerable contribution in the early stages of the project.

Available from:

NASA Center for AeroSpace Information
7121 Standard Drive
Hanover, MD 21076-1320
301-621-0390

National Technical Information Service
5285 Port Royal Road
Springfield, VA 22161
703-605-6000

This report is also available in electronic form at <http://ston.jsc.nasa.gov/collections/TRS/>

Table of Contents

1.0	Introduction	1
2.0	Overview	2
2.1	Regression Analysis	3
2.2	Satellite Tracking Rates.....	10
2.2.1	SSN Composition and Characteristics (Reference 4).....	10
2.2.2	Determining SSN Observation Rate	11
2.3	Estimated Satellite Tracking.....	12
2.3.1	Radar Observation Rates for LEO and DSP	12
2.3.2	Optical Observation Rate for DSP	14
2.3.3	Tracking Summary.....	15
2.4	Determination of Covariance Distribution over the Debris Population.....	15
2.4.1	ISS Altitude Flux	15
2.4.2	Flux Determination Parameters.....	18
2.4.3	Determination of EDR	19
2.4.4	Covariance Distribution.....	19
2.5	Determination of Maneuver Rate and Risk Reduction	21
2.6	Discussion	26
3.0	References	27
	Appendix 1. Comparison of Filtered SATRAK Output to Real-World Tracking.....	28
	Appendix 2. Relation between Object Size and Radar Cross Section	29
	Appendix 3. Derivation of EDR as a Function of Time Derivative of Mean Motion.....	31
	Appendix 4. Flux, EDR and Tracks per Day for 11/9/98 Tracked LEO Objects	32
	Appendix 5. Flux, EDR and Tracks per Day for 11/9/98 Tracked DSP Objects.....	34

Tables

Table 1.1 Coefficients for Equation 1.1 for 8-hour Propagated Covariance.....	3
Table 1.2 Normalized Coefficients for Covariance Determination.....	4
Table 1.3 Regression Analysis Parameters	5
Table 2.1 Space Surveillance Sensor Locations, Types, and Detection Ranges	11
Table 3.1 SSN LEO Sensor Characteristics.....	12
Table 3.2 SSN DSP Radar Sensor Characteristics.....	13
Table 3.3 Deep Space Optical Sensors.....	14
Table 4.1 Weighted distribution of relative angle coefficients for 11/9/98 LEO and DSP catalogs.....	18
Table 4.2. Eight Hour Propagated Covariances.....	20
Table 5.1 Combined maneuver rate, vehicle collision probability (#HITS) and fractional residual risk (FRR) for given Pm values.....	24
Table A.1 Comparison of Actual Tracks to Predicted Tracks for 108-day Period	28

Figures

Figure 2.1 Comparison of normalized radial LEO position uncertainty data from Reference 3 and the fit using the parameters in Table 1.2.	7
Figure 1.2 Comparison of normalized down track LEO position uncertainty data from Reference 3 and the fit using the parameters in Table 1.2.....	7
Figure 1.3 Comparison of normalized radial DSP position uncertainty data from Reference 3 and the fit using the parameters in Table 1.2.	8
Figure 1.4 Comparison of normalized down track DSP position uncertainty data from Reference 3 and the fit using the parameters in Table 1.2.....	8
Figure 1.5 Comparison of normalized cross track position uncertainty predictions, for 8-hr propagation, with LEO and DSP data from Reference 3, using the parameters in Table 1.2.....	9
Figure 5.1 Collision probability versus annual maneuver rate for 8 and 24-hour propagation.....	24
Figure A.1 Experimental mean RCS to wavelength data from Reference 8.	29
Figure A.2 Fit from Reference 8 is indicated by solid curve and fit for this work to the region between $\lambda/D=1$ and $\lambda/D=22$, is shown by the dotted line. In this work, for values $\lambda/D>1$, the optical expression is used, and for values $\lambda/D<0.22$ the Rayleigh expression is used. The 2 vertical dotted lines indicate $\lambda/D=1$ and $\lambda/D<0.22$	30

Acronyms

ISS	International Space Station
DSP	deep space
EDR	energy dissipation rate
LEO	low Earth orbit
NAVSPASUR	Naval Space Surveillance
RCS	radar cross section
SSE	Sum of Squared Errors
SSN	Space Surveillance Network
SSR	Sum of Squares
SST	Sum of Squares Total
TCA	time of closest approach
TPD	tracks per day
USSPACECOM	United States Space Command

1.0 INTRODUCTION

The decision for the International Space Station (ISS) to perform a maneuver to avoid orbital debris will be based upon a predicted collision probability (References. 1, 2). The collision probability will be calculated using real-time best estimates of the debris and ISS position state and position error covariance, propagated to the anticipated time of conjunction, or time of closest approach (TCA). If the computed collision probability exceeds a threshold value, the Red Threshold, a maneuver will be performed unless prevented by other operational considerations. The debris position and its uncertainty, propagated to TCA, will be supplied by United States Space Command (USSPACECOM), by processing observations from its Space Surveillance Network (SSN). For debris avoidance purposes, the ISS will depend initially upon USSPACECOM for its state vectors and covariances, prior to having functional Global Positioning System capability.

It was shown in Reference 1 that, given the distribution of position errors for a space vehicle and the debris population, it is possible to calculate both the anticipated maneuver rate and the residual risk resulting from the choice of a maneuver threshold. The lower the probability threshold, the more maneuvers will be performed. However, no matter how many maneuvers are performed, risk can never be completely eliminated. Further, the performance of a debris avoidance maneuver disrupts the operation of the ISS micro-gravity laboratory and also complicates altitude management for ISS. Clearly the need is to achieve the maximum possible risk reduction while maintaining a sustainable maneuver rate.

2.0 OVERVIEW

Determination of the Red Threshold began with an analysis of data collected in a 1997 study performed by Kaman Sciences Corporation (Reference 3). This study collected and analyzed satellite tracking data from the USSPACECOM Space Surveillance Network (SSN) in order to determine 1) the accuracy with which the system can maintain and predict debris location and 2) how well the system can estimate this accuracy. The satellites chosen for the study spanned the ranges of eccentricities, orbital inclinations and atmospheric drag of the orbiting objects crossing the ISS altitude.

Empirical expressions for the network tracking uncertainty for an object were derived in terms of the number of tracks per day the SSN could provide on an object and the atmospheric drag experienced by the object. The orbiting objects with periods of less than 220 minutes are said to be in low Earth orbit (LEO objects) and the objects with periods 220 minutes or more are said to be in deep space orbits (DSP objects). The LEO and DSP objects were analyzed separately. This process is described in Section 1 of this report.

Section 2 describes how the total possible observation rates for the LEO and DSP objects were determined with the USSPACECOM program SATRAK. This was done using a catalog of element sets of orbiting objects for 11/9/98 obtained from the JSC Space and Life Sciences Directorate.

Section 3 explains how probable observation rates were determined from the SATRAK observation rates.

Section 4 details the process followed to determine covariances for each object. From the observation rate and the drag effect calculated from the orbital element set, an 8-hour propagated covariance was estimated for each LEO and DSP object. This 8-hour covariance was scaled to obtain a 24-hour covariance. The population was divided into 15 groups of comparable position accuracy and the weighted mean covariance was determined for each group.

In Section 5, the maneuver rate and risk reduction associated with each of the 15 groups was determined, using the method of Reference 1, for a complete range of possible maneuver thresholds. The results for each of the 15 groups were combined to produce a total maneuver rate and an aggregate residual risk.

2.1 Regression Analysis

This section describes the empirical regression process, using data from Reference 3, by which the position uncertainty was estimated in terms of tracks per day and the atmospheric drag for the object. This was done for an 8-hour propagation, then scaled to get a 24-hour propagation estimate.

Reference 3 contains metric tracking accuracy information for 63 orbiting objects tracked by the SSN for a period of 108 days and, for each object over the observation period, tabulates the mean observation rate in tracks per day (TPD) and the mean energy dissipation rate (EDR) in watts/kg from atmospheric drag. The metric accuracy data were obtained by comparison of tracking results over a reference time period with a continuous tracking best estimated trajectory, and by comparing abutments of 'independent' orbit determination periods. Reference 3 also contains data relating the uncertainty estimate of the orbit determination process to the observed metric uncertainty in terms of ratios.

Reference 6 carried out an empirical analysis in which these ratios were estimated as a hyperbolic function of $\log_{10}(\text{EDR})$. Equation 1.1 shows the parametric form of the hypothesized relation between standard deviation performance factor (ratio) ρ and EDR. The three parameters to be determined are represented by A_1 , A_2 and A_3 .

$$\rho = (A_2 \log_{10}(\text{EDR}) + A_1) / 2 + \sqrt{\left(\frac{A_2 \log_{10}(\text{EDR}) + A_1}{2}\right)^2 - A_2 \log_{10}(\text{EDR}) - A_3} \quad (1.1)$$

Table 1.1 shows the 8-hour propagated covariance fit parameters, A_1 , A_2 and A_3 , for radial (U), down track (V) and cross track (W) fits to the proposed relation.

Table 1.1 Coefficients for Equation 1.1 for 8-hour Propagated Covariance

	Radial (U)	Down track (V)	Cross track (W)
A_1	11.1665	13.3940	5.3819
A_2	5.0039	5.0994	2.5926
A_3	8.9142	11.2155	4.0113

The metric accuracy data were fit to an expression of the form

$$\sigma = \rho \left[B_1 \left(\frac{1}{\sqrt{TPD}} \right)^2 + B_2 \left(\frac{1}{\sqrt{TPD}} \right)^5 + B_3 \cdot \text{EDR} \right] \quad (1.2)$$

The coefficients B_1 , B_2 , and B_3 were determined by the standard linear least squares technique:

$$\begin{aligned} \bar{\mathbf{x}}\mathbf{B} &= \bar{\mathbf{y}} \\ \bar{\mathbf{x}}^T\bar{\mathbf{x}}\mathbf{B} &= \bar{\mathbf{x}}^T\bar{\mathbf{y}} \end{aligned} \quad (1.3)$$

$$\bar{\mathbf{B}} = (\bar{\mathbf{x}}^T \bar{\mathbf{x}})^{-1} \bar{\mathbf{x}}^T \bar{\mathbf{y}}$$

where

$$\bar{\mathbf{x}} = \left[\left(\frac{1}{\sqrt{TPD}} \right)^2, \left(\frac{1}{\sqrt{TPD}} \right)^5, EDR \right] \quad (1.4)$$

is a matrix,

$$\bar{\mathbf{B}} = \begin{bmatrix} B_1 \\ B_2 \\ B_3 \end{bmatrix} \quad (1.5)$$

is a vector, and $\bar{\mathbf{y}}$ is the vector of position uncertainties for the individual objects from Reference 3. Radial, down track and cross track data were fit separately and the coefficients B_1 , B_2 , B_3 were determined for each. The down track data spanned 3 orders of magnitude and the linear fit poorly tracked the low covariances. For the LEO down track data, a weighted least squares scheme was used:

$$\bar{\mathbf{x}}^T w \bar{\mathbf{x}} \bar{\mathbf{B}} = \bar{\mathbf{x}}^T w \bar{\mathbf{y}}$$

$$\bar{\mathbf{B}} = (\bar{\mathbf{x}}^T w \bar{\mathbf{x}})^{-1} \bar{\mathbf{x}}^T w \bar{\mathbf{y}} \quad (1.6)$$

where

$$w = \begin{pmatrix} 1/y_1 & 0 & \dots & 0 \\ 0 & 1/y_2 & \dots & 0 \\ \cdot & \cdot & \dots & \cdot \\ \cdot & \cdot & \dots & \cdot \\ 0 & 0 & \dots & 1/y_n \end{pmatrix} \quad (1.7)$$

This ad-hoc procedure produced the desired fit, though the residuals were slightly higher than for the unweighted procedure. Table 1.2 shows the parameters of equation 1.2 employed in this analysis for LEO and DSP objects.

Table 1.2 Normalized Coefficients for Covariance Determination

	LEO			DSP		
	B ₁	B ₂	B ₃	B ₁	B ₂	B ₃
U	78.6696	49.4403	54.5407	11.2429	7.0571	7.7857
V	25.5104	61.5031	90.4592	10.455	4.335	15.3680
W	71.9077	-51.6531	4.46802	12.7383	8.8083	4.40231

Analysis of Variance summation parameters associated with the LEO and DSP fits are shown in Table 1.3. Figures 1.1, 1.2, 1.3, 1.4, and 1.5 show the fits to the normalized data. The structure of the data is well described by the fits. Only the deep space cross track data shows appreciable deviation from the fit. The deep space flux (see Section 4) comprises only about 4% of the total debris flux seen by ISS and the cross track position uncertainty has little effect on the collision probability because of the large down track uncertainty dominates in most physically possible conjunctions.

The Sum of Squares Total (*SSTO*), Regression Sum of Squares (*SSR*) and Sum of Squared Errors (*SSE*) are defined as

$$SSTO = \bar{y}^T \bar{y} - \frac{1}{n} \left(\sum_{i=1}^n y_i \right)^2, \quad (1.8)$$

$$SSR = B\bar{x}^T \bar{y} - \frac{1}{n} \left(\sum_{i=1}^n y_i \right)^2, \quad \text{and} \quad (1.9)$$

$$SSE = (\bar{y} - \bar{x}B)^T (\bar{y} - \bar{x}B) \quad (1.10)$$

Table 1.3 Regression Analysis Parameters

	<i>SSTO</i>	<i>SSR</i>	<i>SSE</i>	R^2
Radial LEO	65240.9	63322.4	1918.5	0.971
Down Track LEO*	188136.5	180092.6	3532.7	0.983
Cross Track LEO**	2489.9	2351.4	138.4	0.944
Radial DSP	583.14	479.134	251.4	0.8214
Down Track DSP	9253.0	8736.6	192.2	0.944
Cross Track DSP	291.5	220.1	71.4	0.755

* Weighted least squares used.

** One data point dropped from fit as outlier.

Because of the weighting of measurements in the fitting process, the equation $SSTO=SSR+SSE$ is not strictly valid. Rather $SSTO=SSR+SSRD+SSE$, where $SSRD = 1241.5$ is the unmodeled effect of weighting. Still $R^2 = SSR / SSTO$ is a valid assessment of the fraction of the effects in the data that are modeled. The R^2 value of 0.971 indicates excellent modeling.

By comparison of the 8-hour propagated uncertainties to the 24-hour propagated uncertainties, it was estimated that the radial uncertainty at 24 hours is twice that at 8 hours, that the down track uncertainty is three times that at 8 hours, and that the cross track uncertainty is about 1.5 time that at 8 hours. The 8-hour results were multiplied by these factors to obtain the 24-hour estimates.

It should be noted that for moderate tasking, the empirical position uncertainties determined in this analysis depend almost entirely on EDR, with minor dependence on TPD.

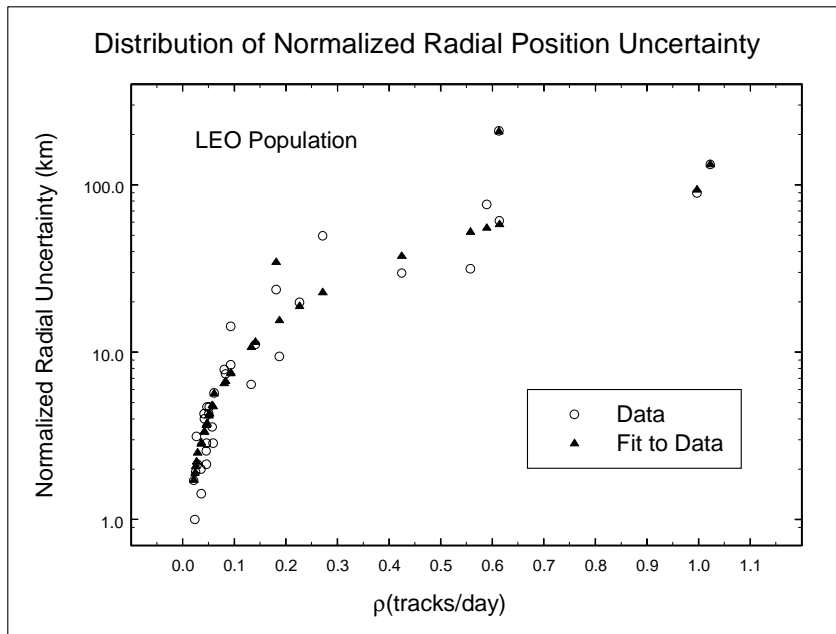


Figure 1.1 Comparison of normalized radial LEO position uncertainty data from Reference 3 and the fit using the parameters in Table 1.2.

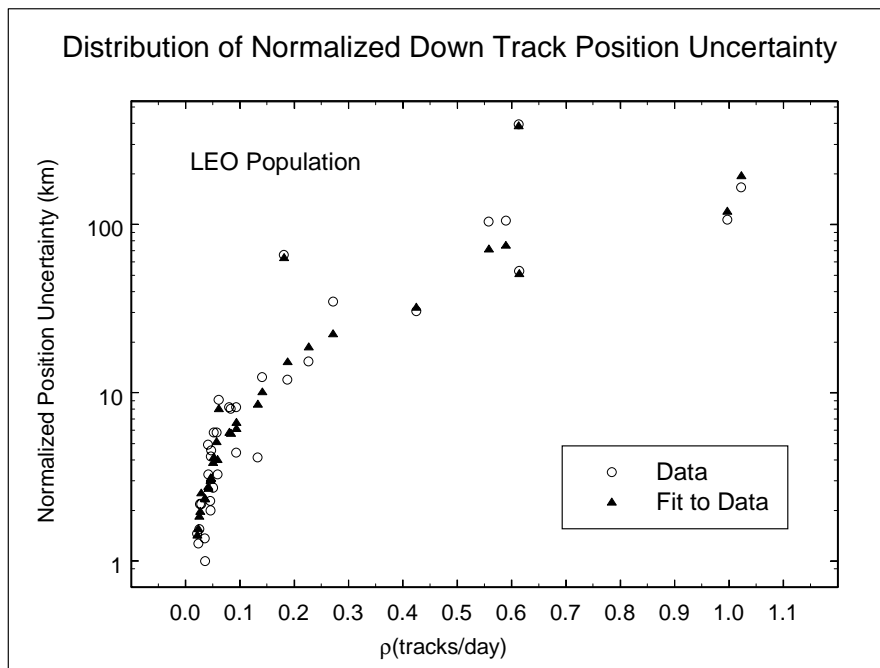


Figure 1.2 Comparison of normalized down track LEO position uncertainty data from Reference 3 and the fit using the parameters in Table 1.2.

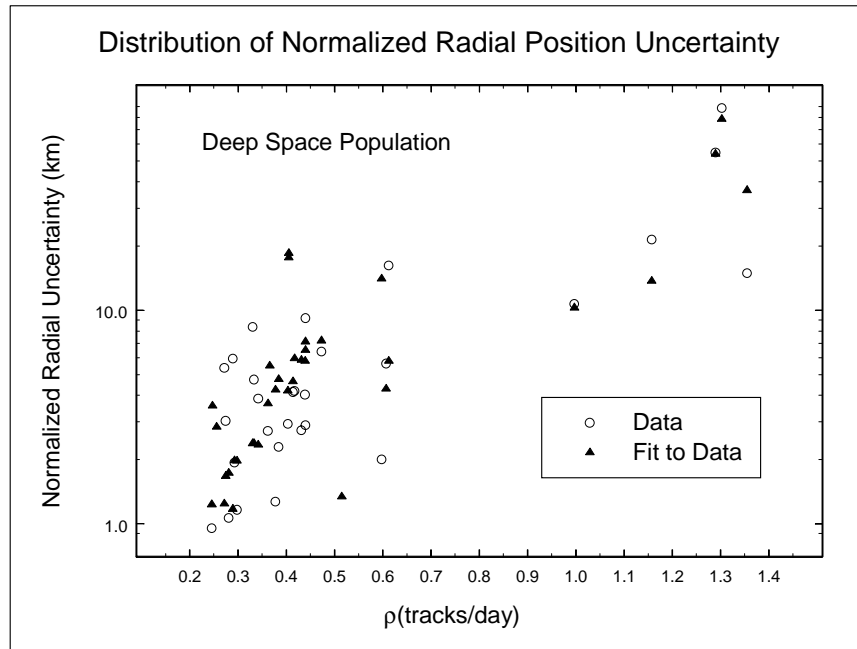


Figure 1.3 Comparison of normalized radial DSP position uncertainty data from Reference 3 and the fit using the parameters in Table 1.2.

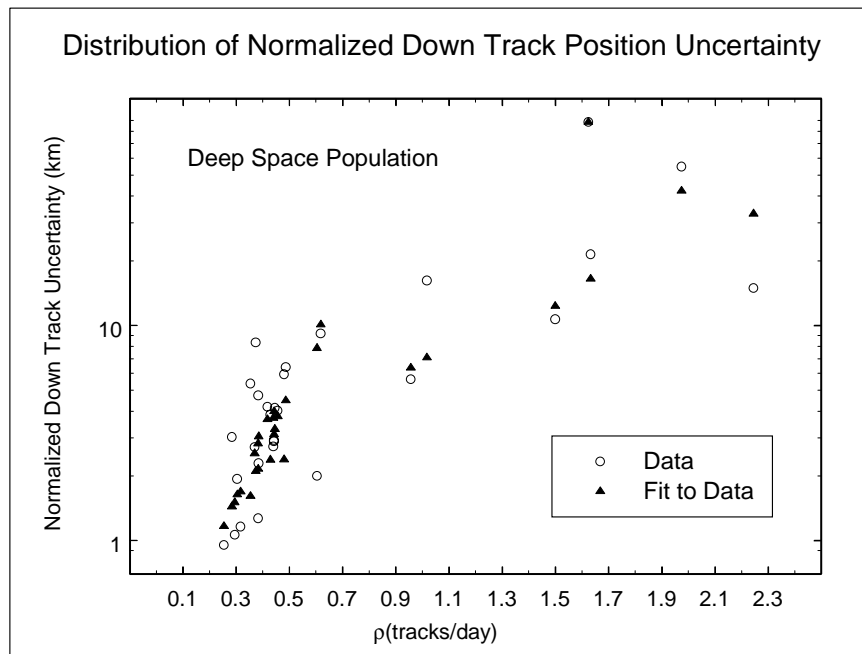


Figure 1.4 Comparison of normalized down track DSP position uncertainty data from Reference 3 and the fit using the parameters in Table 1.2.

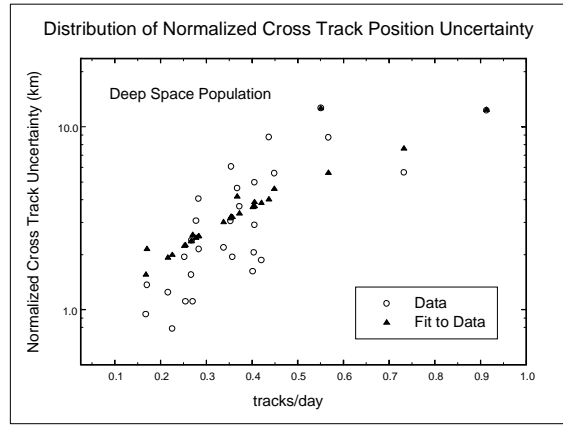
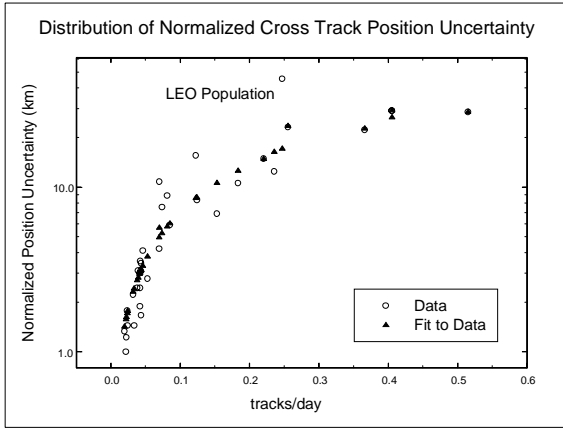


Figure 1.5 Comparison of normalized cross track position uncertainty predictions, for 8-hr propagation, with LEO and DSP data from Reference 3, using the parameters in Table 1.2.

2.2 Satellite Tracking Rates

The quantity and distribution of satellite tracking positional data affects the accuracy of orbit determination. The regression analysis in Section 1 relates the accuracy of orbit determination to tracks per day and EDR. This section describes how the tracking rate and tracking distance for each cataloged object crossing the ISS altitude band was estimated. Whether or not the “tracked” object was actually detectable is dealt with in Section 3.

2.2.1 SSN Composition and Characteristics (Reference 4)

The SSN consists of 31 Department of Defense and privately owned radar and optical sensors at 15 worldwide locations, a communications network, and primary and alternate operations centers for data processing. Most of the sensors are mechanical tracking, phased-array, and continuous-wave radars; optical telescopes are also used.

Each type of sensor contributes data in a manner unique to its characteristics. Mechanical tracking radars can provide precision metric data, phased array radars can furnish large daily volumes of tracking data, and the Navy Space Command radar fence can provide valuable information on satellite maneuvers and fragmentations. However, even sensors of a given type, e.g., phased array radars, may possess different capabilities due to their locations or physical characteristics.

Both mechanical trackers and phased-array radars are capable of providing continuous arc tracking. A continuous-wave radar system, which cannot provide continuous arc tracking, consists of several transmitters and receivers, each placed in a different physical location across a plane. The continuous wave Naval Space Surveillance System consists of six receivers and three transmitters located at sites from California to Georgia. Optical telescope tracking is used primarily for deep space satellites.

The various network sensors' support to the space surveillance mission are categorized as being dedicated, collateral, or contributing. Dedicated sensors support the space surveillance mission as their primary purpose. Collateral sensors primarily support other missions, such as ballistic missile warning or launch vehicle range support, but also provide space surveillance capabilities. Contributing sensors are used under a contract or an agreement to support the space surveillance mission only when requested.

Over one-third of the network sensors provide data on space objects only in near-Earth altitudes (5,875 kilometers and less), about one-third only in deep space, and the remainder in both near-Earth and deep space. Table 2.1 lists the network sensors by category, with the sensor types and detection ranges by locations.

Table 2.1 Space Surveillance Sensor Locations, Types, and Detection Ranges

Sensor location	Sensor type	Sensor detection range
Dedicated support		
Eglin Air Force Base, Florida	1 Phased-array radar	Near-Earth & deep space
Diego Garcia, Indian Ocean (GEODSS)	3 Telescopes	Deep space
Maui, Hawaii (GEODSS)	6 Telescopes	4 Deep space and 2 near-Earth and deep space
Socorro, New Mexico (GEODSS)	3 Telescopes	Deep space
Western and southern U.S. Naval Space Surveillance System (NAVSPASUR)	1 Continuous-wave radar system	Near-Earth
Collateral support		
Antigua, British West Indies	1 Mechanical tracker radar	Near-Earth
Ascension Island, South Atlantic Ocean	2 Mechanical tracker radar	Near-Earth
Beale AFB, California (PAVE PAWS-WEST)	1 Phased-array radar with 2 faces	Near-Earth
Cape Cod Air Force Station, Massachusetts (PAVE PAWS-EAST)	1 Phased-array radar with 2 faces	Near-Earth
Cavalier Air Force Station, North Dakota (PARCS)	1 Phased-array radar	Near-Earth
Clear Air Station, Alaska (BMEWS)	1 Mechanical tracker radar	Near-Earth
Fylingdales, England (BMEWS)	1 Phased-array radar with 3 faces	Near-Earth
Kaena Point, Oahu, Hawaii	1 Mechanical tracker radar	Near-Earth
Thule, Greenland (BMEWS)	1 Phased-array radar with 2 faces	Near-Earth

Near-Earth sensors are used exclusively on LEO objects; deep space sensors, optical and radar exclusively for DSP objects.

2.2.2 Determining SSN Observation Rate

Most sensors are not dedicated to the space surveillance mission. It would be a false to assume that a sensor provides positional data on a satellite every time it is in coverage. Only for special satellites is a sensor tasked by the Cheyenne Mountain Space Control Center to obtain data on every available pass; even then, tracking opportunities may be missed in favor of higher priority satellites. Additionally, whether or not an object is observable by radar depends upon the signal to noise ratio for the reflected signal, determined by the radar cross section for the object, the distance at which the object was detected and the electronic ‘gain’ characteristics of the sensor. Whether or not an object is observed optically depends on the optical magnitude of the object and requires that the sensor be in darkness. The optical magnitude depends on the size, and albedo of the object and upon the solar phase angle.

In Reference 3, the amount of tracking is less than the predicted amount. We assume in this work that an ISS conjunction will have sufficiently high priority that essentially all observable passes will be tracked.

2.3 Estimated Satellite Tracking

Using program SATRAK, as described in Section 2, the tracking opportunities were separately determined for the LEO radar sites, the DSP radar sites, and the DSP optical observing sites. We assumed that only the LEO sites observed LEO objects and only the DSP sites observed DSP objects. In this section we describe how the signal to noise ratio, S/N, for the radars, and the visual magnitude, M, for the optical sensors were estimated

2.3.1 Radar Observation Rates for LEO and DSP

The SATRAK calculations described in Section 2 output was filtered by applying sensor gain and wavelength, estimated radar cross section of each object, and the range at time of observation. These parameters were used to calculate a signal to noise ratio for each observation opportunity.

The JSC Space and Life Sciences Directorate maintains a catalog of radar cross section (RCS) and estimated physical mean diameter for most of the cataloged debris population. The tabulated RCS values are for a wavelength of 0.68 meters, the wavelength of most of the sensor network. If the wavelength of the sensor is 0.68 meters, then the tabulated RCS is used without modification. If the wavelength of the sensor is other than 0.68 meters, the radar cross section must be corrected for the individual sensor. Table 3.1 shows the SSN LEO radar characteristics. Table 3.2 shows the SSN DSP radar characteristics. The SSN DSP sensors operate on a slower duty cycle when tracking objects beyond a range 5000 km and have a larger open loop gain for objects beyond that range.

The Naval Space Surveillance (NAVSPASUR) fence measurements were not included in either the LEO or DSP calculations because of the extremely poor associated metric accuracy. The utilization factor for the Millstone DSP sensor was assumed to be one even though the utilization factor for the Kaman Sciences study (Reference 3) was very low. (See Appendix 1)

Table 3.1 SSN LEO Sensor Characteristics

Shown are sensor number and name, Gain (G), Wavelength (λ), and Max Range.

Sensor	Name	G (dB)	λ (meters)	Max Range (km)
344	Fylingdales	282	0.68	6000
354	Ascension	263	0.053	4910
359	Clear	277	0.68	4910
363	Antigua	258	0.053	4910
386	Cape Cod	277.6	0.68	5555
388	Beale	277	0.68	5555
393	Cobra Dane	300	0.23	
394	Thule	282	0.68	5555
396	PARCS- Cavalier	278	0.68	3300
399	Eglin	281	0.68	13210
932	Kaena Point	277	0.053	6380

Table 3.2 SSN DSP Radar Sensor Characteristics.

Shown are sensor number and name, Wavelength (λ), Gain Change Range, low altitude Sensor Gain (G1), and high altitude Sensor Gain (G2) .

Sensor	Name	λ (meters)	Gain Change Range (km)	G1 (dB)	G2 (dB)
334	Altair	0.68	5000	277.5	309
398	Eglin	0.68	5000	291	314
369	Millstone	0.68	5000	286.5	319

For a sphere of diameter D, and a sensor of wavelength λ , Equations 3.1, 3.2, and 3.3 relate the physical diameter to the radar cross section. If an object was not in the RCS catalog, an RCS of 1m^2 was assumed. There are 3 wavelength regions of interest: the optical, the Mie, and the Rayleigh. Equation 3.1 represents the relationship for optical wavelengths. Equation 3.2 is the well-known Rayleigh scattering cross section. A derivation of Equation 3.3, an interpolation between the optical region and the Rayleigh region, is found in Appendix 2.

$$\text{if } \frac{D}{\lambda} \geq 1 \quad \text{then} \quad RCS = \frac{\pi D^2}{4} \quad (\text{optical region}) \quad (3.1)$$

$$\text{if } \frac{D}{\lambda} \leq 0.22 \quad \text{then} \quad RCS = \lambda^2 \left(\frac{9\pi^5}{4} \right) \left(\frac{D}{\lambda} \right)^6 \quad (\text{Rayleigh region}) \quad (3.2)$$

$$\text{if } 1 \geq \frac{D}{\lambda} \geq 0.22 \quad \text{then} \quad RCS = 0.7853982 \lambda^2 \left(\frac{D}{\lambda} \right)^{1.524721} \quad (\text{Mie region}) \quad (3.3)$$

The signal to noise ratio for a sensor will follow the equation

$$\frac{S}{N} = G \frac{RCS}{R^4} \quad , \quad (3.4)$$

where R is the range, in meters, to the object and G, the ‘gain,’ is a constant associated with the sensor involving the characteristics of the electronics of the sensor. The units of RCS are meters squared.

Defining $10 \log_{10}(A)$ to be A_{DB} , equation 3.4 becomes

$$\left(\frac{S}{N} \right)_{DB} = G_{DB} + 10 \log_{10}(RCS) - 40 \log_{10}(R) \quad . \quad (3.5)$$

The G_{DB} are tabulated for the sensors. In this study we employed a detection threshold of

$$\left(\frac{S}{N}\right)_{DB} = 12 \quad . \quad (3.6)$$

This corresponds to a numeric $\frac{S}{N}$ value of 15.8. For lower values, the time resolution will begin to be adversely affected. However, as noted in Section 1, there is not a large dependence on TPD in the empirically determined position uncertainties.

2.3.2 *Optical Observation Rate for DSP*

The visual magnitude, M , for an object is assumed to depend on object diameter, D , in cm; albedo, A ; range R in km; and solar phase angle, ϕ , in radians; as

$$M = -26.74 - 2.5 \log_{10} \left\{ \frac{AD^2}{4} \cdot (\sin(\phi) + (\pi - \phi) \cdot \cos(\phi)) - \frac{3}{2} \pi R^2 \cdot 10^6 \right\} \quad (3.7)$$

The values of D are taken from the Space and Life Science's RCS Table, R and ϕ from the SATRAK output and the albedo is assumed to be 0.1, an approximate average value.

We assume only one observation track per satellite pass, and find the lowest value of M for the pass. Table 3.3 shows the optical sensors used in the SATRAK calculations.

Table 3.3 Deep Space Optical Sensors.

Sensor	Name	Max Range (km)
212	Socorro	none
232	Maui	none
242	Diego Garcia	none

Based on private communication from several sources, the detection threshold magnitude was taken to be

$$M = 16. \quad (3.8)$$

2.3.3 Tracking Summary

We have assumed that all tracking passes with a radar S/N ratio of 12dB, either of LEO or DSP objects, and all optical passes for DSP objects with an visual magnitude of 16 or less will result in an observed track. Comparing the observation rates determined in this work with those of the Kaman Sciences Study, the observation rates are about 50% greater for the LEO objects and about twice those for the DSP objects. The priority assigned by the SSN to the Kaman Study data acquisition was relatively low. Given a priority appropriate for the protection of a national asset, the track observation rate in this report is justified.

2.4 Determination of Covariance Distribution over the Debris Population

This section details the process followed to determine the covariances distribution. The flux associated with each object with respect to a reference object orbiting at ISS altitude, was determined using a statistical method developed by Kessler (Reference 5). The observation rate was determined for each object using the method described in Section 3. From two catalogs of orbital elements, about three weeks apart (10/26/98 and 11/9/98), the drag effect, or EDR was calculated from the difference in the orbital elements. Using the observation rate and EDR, an 8-hour propagated covariance was estimated for each LEO object, following the method of Section 2. The LEO population was divided into 15 bins of comparable down track position accuracy and the weighted mean covariance was determined for each group. Objects determined to be attached to Mir were removed from the catalog in the flux computation.

A total debris flux of about 0.26 objects / km² / year was observed at 400 km using the method of Kessler (Reference 5). USSPACECOM classifies those objects having an orbital period of less than 220 minutes as being in LEO and those having a longer orbital period as having ‘deep space’ orbits. The flux associated with LEO objects crossing the 400 km altitude was 0.25 objects / km² / year.

2.4.1 ISS Altitude Flux

Kessler derived a statistical method to determine the mean flux of an orbiting object seen by a ‘target’ object in a circular orbit at a fixed orbital inclination. The individual fluxes can be added to produce a total flux seen by the target object. This was the basis for the development of the JSC Flux Model (Reference 7). Reference 5 contains a detailed derivation of Kessler’s method, which is described below.

The average flux seen by orbiting object 0, due to orbiting object k is

$$FLUX = \iint_{r,\beta} S_0(r, \beta, i_0) S_k(r, \beta, i_k) V^{rel} 2\pi r^2 \cos(\beta) dr d\beta \quad , \quad (4.1)$$

where $S_0(r, \beta, i_0)$ and $S_k(r, \beta, i_k)$ are the spatial densities associated with the orbits of target and conjuncting objects, V^{rel} is the magnitude of the relative velocity between the two objects, and r and β are the radius and latitude of the differential. The expression assumes that an averaging over a large number of cycles of argument of perigee and right ascension of ascending node has occurred. The radial and angle dependent parts of $S_0(r, \beta)$ and $S_k(r, \beta)$ may be

separated into radial and latitude dependent functions as $S_0(r, \beta) = s_0(R, q_0, q'_0) f_0(\beta, i_0)$ and $S_k(r, \beta) = s_k(R, q_k, q'_k) f_k(\beta, i_k)$, and an average value computed for each component over a range of radius R and latitude β , thus removing singularities. Here q and q' are perigee and apogee, and i is the orbital inclination. Average values are

$$\bar{s}_0 = \frac{1}{4\pi\bar{R}^2\Delta R} \quad , \quad (4.2)$$

assuming a circular orbit, where ΔR is the thickness of the radial shell containing the ISS orbit. Averaging over radius,

$$\bar{s}_k(R, q, q') = \frac{1}{4\pi^2 a_k \bar{R} \Delta R} \sin^{-1} \left(\frac{2R - q - q'}{q' - q} \right) = \frac{1}{4\pi^2 a \bar{R} \Delta R} (F_1(R', q, q') - F_2(R, q, q')) \quad (4.3)$$

Avoid singularities at apogee and perigee,

$$\begin{aligned} F_1 &= \sin^{-1} \left(\frac{2R' - 2a}{q' - q} \right) \quad \text{if } q < R' < q' \quad , \\ F_1 &= \frac{\pi}{2} \quad \text{if } R' > q' \quad , \\ F_1 &= -\frac{\pi}{2} \quad \text{if } R' < q \quad , \end{aligned} \quad (4.4)$$

and

$$\begin{aligned} F_2 &= \sin^{-1} \left(\frac{2R - 2a}{q' - q} \right) \quad \text{if } q < R < q' \quad , \\ F_2 &= -\frac{\pi}{2} \quad \text{if } R < q \quad , \\ F_2 &= \frac{\pi}{2} \quad \text{if } R > q' \quad , \end{aligned} \quad (4.5)$$

Averaging over latitude,

$$\bar{f}(\beta, \beta', i) = \frac{2}{\pi} \left(\frac{G_1(\beta', i) - G(\beta, i)}{\sin \beta' - \sin \beta} \right) \quad , \quad (4.6)$$

where

$$G_1 = \sin^{-1}\left(\frac{\sin \beta'}{\sin i}\right) \text{ if } \beta < i \quad , \quad G_1 = \frac{\pi}{2} \text{ if } \beta' \geq i \quad , \quad (4.7)$$

and

$$G_2 = \sin^{-1}\left(\frac{\sin \beta}{\sin i}\right) \text{ if } \beta < i \quad , \quad G_2 = \frac{\pi}{2} \text{ if } \beta \geq i \quad . \quad (4.8)$$

The numerical integral is evaluated as

$$FLUX_K = \sum_j \bar{s}_0(\bar{R}) \bar{s}_k(\bar{R}, q, q') \bar{f}_0(\bar{\beta}_j, i_o) \bar{f}_k(\bar{\beta}_j, i_k) \bar{V}^{rel} 2\pi \bar{R}^2 \cos \beta_j \Delta R \Delta \beta \quad (4.9)$$

with the sum over the increments of β_j .

The relative velocity is defined as $\bar{V}^{rel} = \bar{V}_k - \bar{V}_0$. The mean relative velocity associated with a conjunction increment in the above expression is

$$\bar{V}^{rel} = \sqrt{V_o V_k \cos \gamma_o \cos \gamma_k \cos \alpha_o \cos \alpha_k} \quad , \quad (4.10)$$

where α is the angle the orbit makes with respect to a line of constant latitude and γ is the angle the orbit makes with respect to a plane tangent to the surface of the Earth.

$$\cos \alpha = \frac{\cos i}{\cos \beta} \quad \text{and} \quad \cos \gamma = \sqrt{\frac{qq'}{R(2a - R)}} \quad . \quad (4.11)$$

There are, in fact, two possible relative velocities for each conjunction increment, given by

$$V_1^{rel} = \sqrt{V_o^2 + V_k^2 - 2V_o V_k \cos \gamma_o \cos \gamma_k \cos(\alpha_o + \alpha_k)} \quad (4.12)$$

and

$$V_2^{rel} = \sqrt{V_o^2 + V_k^2 - 2V_o V_k \cos \gamma_o \cos \gamma_k \cos(\alpha_o - \alpha_k)} \quad . \quad (4.13)$$

The angular distribution of the debris with respect to the velocity vector of the target object (ISS) is needed for the calculations of Section 5. We have defined $\bar{V}^{rel} = \bar{V}_k - \bar{V}_0$, and thus

V_{rel} , V_0 , and V_k form a triangle. By the law of cosines, $\cos A = \frac{c^2 + b^2 - a^2}{2bc}$, the angle between V_{rel} and V_0 , ϕ^{rel} , is

$$\cos(\phi_{0k}^{rel}) = \frac{V_{rel}^2 + V_0^2 - V_k^2}{2V_{rel}V_0} \quad . \quad (4.14)$$

This equation can be solved for the relative angle ϕ^{rel} as

$$\phi_{0k}^{rel} = \cos^{-1}\left(\frac{V_0^2 + V_k^2 - V_{rel}^2}{2V_0V_k}\right) \quad . \quad (4.15)$$

The angular distribution is given by

$$D(\phi_i) = \frac{n(\phi_i)}{\sum_i n(\phi_i)} \quad , \quad (4.16)$$

where, if $(\phi_{jk} - 7.5^\circ) \leq \phi_i < (\phi_{jk} + 7.5^\circ)$, then

$$n(\phi_i) = n(\phi_i) + \bar{s}_0(\bar{R})\bar{s}_k(\bar{R}, q, q')\bar{f}_0(\bar{\beta}_j, i_o)\bar{f}_k(\bar{\beta}_j, i_k)\bar{V}^{rel} 2\pi\bar{R}^2 \cos \beta_j \Delta R \Delta \beta \quad . \quad (4.17)$$

The $D(\phi_i)$ are shown below in Table 4.1 .

Table 4.1 Weighted distribution of relative angle coefficients for 11/9/98 LEO and DSP catalogs.

rel. ang.	0°	15°	30°	45°	60°	75°	90°	105°	120°	135°	150°	165°
$D(\phi_i)$.0000	.0913	.284	.221	.216	.147	.030	.006	.002	.001	.000	.000

By integrating over an 80 km swath, from 440 to 360 km, we are averaging over several months of conjunctions, past and future.

2.4.2 Flux Determination Parameters

The semi-major axis, a , perigee, q , apogee, q' , orbital inclination, i , and eccentricity, e , are needed in the flux determination discussed above. The two-line element (TLE) set, upon which much of our analysis is based, contains orbital inclination, i , eccentricity, e , mean motion, n_0 , and $\frac{\dot{n}_0}{2}$.

The semi-major axis, a , may be determined from the mean motion. The mean motion is defined as

$$n_0 = \sqrt{\frac{\mu_e}{a^3}} \frac{rad}{sec} = \frac{2\pi}{T} \quad , \quad (4.18)$$

where T is the period, and μ_e is the Earth's gravitational constant. In the TLE, the units of mean motion are *orbits per day*. The semi-major axis is calculated as

$$a = \left[\frac{\mu_e}{(2\pi n_0)^2} \right]^{\frac{1}{3}} = \frac{(\mu_e)^{\frac{1}{3}}}{\left(\frac{2\pi n_{SPACECOM}}{86400 \text{ sec / day}} \right)^{\frac{2}{3}}} \quad , \quad (4.18)$$

where $\mu_e = 3.9860 \times 10^5 \text{ km}^3/\text{sec}^2$.

Perigee, q , and apogee, q' , are determined as

$$q = a(1 - e) \quad \text{and} \quad q' = a(1 + e) \quad . \quad (4.19)$$

2.4.3 Determination of EDR

In general, the TLE is determined on a limited amount of data. The $\dot{n}_0/2$ term for a single object is observed to vary considerably from one element set to another, partly because of solution errors (often for low drag objects this term has the wrong sign, indicating energy going into the orbit) and partly because of a varying atmosphere. For this work we seek a mean solution over a span of time. From two catalogs of orbital elements, 19 days apart, the drag effect, or energy dissipation rate (EDR) was calculated from the difference in the mean motion. An invariant semi-major axis is calculated as

$$\tilde{a} = a \left\{ 1 - \frac{3/4 R_e^2 J_2}{a(1 - e^2)^{3/2}} (3 \cos^2(i) - 1) \right\} \quad , \quad (4.20)$$

where the Earth equatorial radius, $R_e = 6378.134$, and $J_2 = 0.00108261$ is the coefficient of the $l=2$ zonal term in the spherical harmonic expansion of the Earth's gravitational potential.

Then

$$EDR = \frac{\mu_e}{2} \left(\frac{1}{\tilde{a}_2} - \frac{1}{\tilde{a}_1} \right) \left(\frac{1}{t_2 - t_1} \right) \quad , \quad (4.21)$$

where t_1 and t_2 are the epoch times for \tilde{a}_1 and \tilde{a}_2 .

If the object does not appear in the 2nd catalog, the EDR is calculated directly from $\frac{\dot{n}_{SPACECOM}}{2}$ as

$$EDR = -\frac{1}{3} \sqrt{\mu_e a} (\dot{n}_0) = -\frac{2}{3} \sqrt{\mu_e a} \left(\frac{2\pi \frac{\dot{n}_{SPACECOM}}{2}}{86400} \right) \quad , \quad (4.22)$$

(see Appendix 3). The results of the EDR computations, as well as flux and tracks per day, for the 11/9/98 LEO catalog objects are presented in Appendix 4.

2.4.4 Covariance Distribution

The flux associated with each object with respect to a reference object orbiting at ISS altitude, was determined using the method outlined above. The radar observation opportunity frequency was determined for each object using the method described in Section 3. The EDR for each object was calculated as indicated above. An 8-hour propagated covariance was estimated for each LEO object, following the method of Section 2 using observation rate and EDR. The LEO population was divided into 15 bins of comparable down track position accuracy and the weighted mean covariance was determined for each group. Weighting was based on the flux associated with each object. Table 4.2 shows the 8-hour propagated covariances and the

associated flux for the 15 down track accuracy bins. The total LEO flux is 0.252 obj / km² / yr. The total DSP flux is 0.014 obj / km² / yr.

Table 4.2. Eight Hour Propagated Covariances

Bin	flux (obj/km ² /yr)	Av. EDR (watts/kg)	σ_U (km)	σ_V (km)	σ_W (km)
1	0.0117	0.0019	0.018	0.143	0.023
2	0.0406	0.0033	0.028	0.229	0.029
3	0.0161	0.0047	0.033	0.314	0.041
4	0.0275	0.0072	0.038	0.395	0.035
5	0.0170	0.0101	0.046	0.534	0.041
6	0.0285	0.0144	0.062	0.765	0.041
7	0.0176	0.0221	0.080	1.04	0.038
8	0.0238	0.0304	0.114	1.50	0.045
9	0.0063	0.0366	0.164	2.07	0.071
10	0.0120	0.0512	0.221	2.83	0.071
11	0.0234	0.0644	0.388	4.65	0.129
12	0.0077	0.111	0.463	6.13	0.111
13	0.0084	0.220	0.883	12.3	0.148
14	0.0113	0.596	2.45	36.4	0.251
15	0.0230	1.65	16.5	203.3	1.21

For 20 objects, 24-hour covariances were available. The average ratios between radial, down track, and cross track sigmas were 2, 3, and 1.5 respectively. Estimates of the 24-hour covariances were obtained by scaling the 8-hour values, by multiplying the radial uncertainty by 2, the down track by 3 and the cross track by 1.5.

The total deep space flux, for the 11/9/98 catalog was calculated to be about 0.001 obj / km² / yr, using the same method used for LEO.

2.5 Determination of Maneuver Rate and Risk Reduction

In this section the maneuver rate and risk reduction associated with each of the 15 satellite groups is determined, using the method of Reference 1, for a complete range of possible maneuver thresholds. The results for each of the 15 groups are combined to produce a total maneuver rate and an aggregate residual risk.

For the purposes of this work we assume the debris conjuncture and the target vehicle travel parallel to the surface of the Earth with the same velocity, and with known state vector uncertainties, which we express in terms of covariance matrices. The spatial part of the covariance matrix for the orbiter and debris conjuncture is taken to be of the form

$$C_{UVW}^{ISS} = \begin{bmatrix} \sigma_{UU}^{ISS} & \sigma_{UV}^{ISS} & 0 \\ \sigma_{VU}^{ISS} & \sigma_{VV}^{ISS} & 0 \\ 0 & 0 & \sigma_{WW}^{ISS} \end{bmatrix} \quad \text{and} \quad C_{UVW}^{deb} = \begin{bmatrix} \sigma_{UU}^{deb} & \sigma_{UV}^{deb} & 0 \\ \sigma_{VU}^{deb} & \sigma_{VV}^{deb} & 0 \\ 0 & 0 & \sigma_{WW}^{deb} \end{bmatrix}, \quad (5.1)$$

$$\text{where } \sigma_{UV} = \rho_{UV} \sigma_U \sigma_V, \quad (5.2)$$

for both the Orbiter and the debris object with ρ the correlation coefficient and

$$\sigma_U = \sqrt{\sigma_{UU}} \quad \text{and} \quad \sigma_V = \sqrt{\sigma_{VV}}. \quad (5.3)$$

Given the angle between orbital planes, θ , the relative angle θ_r , made by the conjuncture as seen by the space vehicle is given by

$$\theta_r = (180 - \theta) / 2. \quad (5.4)$$

Representing the target object as a sphere of radius R , for the conjuncting object at distance R_0 at time of conjunction, the collision probability is

$$P(r < R) = \frac{1}{2\pi \lambda_1 \lambda_2} \int_{r=0}^R \int_{\vartheta=0}^{2\pi} e^{-\frac{(r \cos \vartheta - R_0 \cos \varphi)^2}{2\lambda_1^2}} e^{-\frac{(r \sin \vartheta - R_0 \sin \varphi)^2}{2\lambda_2^2}} r dr d\vartheta, \quad (5.5)$$

where $R_0 = |\bar{R}_{rel}| = |\bar{R}_{rel}^{diag}|$, $\varphi = \tan^{-1}\left(\frac{R_{rel_2}}{R_{rel_1}}\right)$ with λ_1 and λ_2 given by

$$\lambda_{.1} = \frac{Tr(M) + \sqrt{(Tr(M))^2 - 4|M|}}{2} \quad \text{and} \quad \lambda_{.2} = \frac{Tr(M) - \sqrt{(Tr(M))^2 - 4|M|}}{2}. \quad (5.6)$$

Here $Tr(M)$ and $|M|$ are the trace and determinant of the matrix M and λ_1 and λ_2 are the eigenvalues of the matrix M :

$$M = \begin{bmatrix} \sigma_{UU}^{ISS} + \sigma_{UU}^{deb} & (\sigma_{UV}^{ISS} + \sigma_{UV}^{DEB}) \sin(\theta) \\ (\sigma_{VU}^{ISS} + \sigma_{VU}^{DEB}) \sin(\theta) & \sigma_{WW}^{ISS} \cos^2(\theta) + \sigma_{VV}^{ISS} \sin^2(\theta) \end{bmatrix}. \quad (5.7)$$

A line between the target object and the conjuncting object makes an angle φ with the ‘1’ axis, at time of conjunction. The integration variables r and ϑ define a position within the cross section of the target sphere, ϑ being the angle with the ‘1’ axis.

Examining all possible miss distances and all possibilities of conjunction geometry, surfaces of constant collision probability will consist of closed surfaces, centered about the space vehicle. The area associated with the projection of these surfaces in a given direction is represented as an ellipse.

Consider the surface associated with a collision probability P_m , the collision probability threshold for which a maneuver will be performed. Let the area associated with the projection of these surfaces in a given direction be $A_{P_m}(\phi_i^{rel})$ (km²). The debris flux, for an accuracy bin of Table 4.2, from direction ϕ_i^{rel} , over our 15° interval, is $f(\phi_i^{rel}) = flux D(\phi_i^{rel})$ (obj / km² / yr), where *flux* comes from Table 4.2 and $D(\phi_i^{rel})$ is the directional coefficient from Table 4.1, determines the maneuver rate for objects coming from that direction. The $f(\phi_i^{rel})$ are obtained from Table 4.2. This product, summed over the angle increments, gives the total annual maneuver rate:

$$N_m = \sum_i f(\phi_i^{rel}) A_{P_m}(\phi_i^{rel}) \quad . \quad (5.8)$$

For a vehicle of cross section $A_{\otimes}(\phi_i^{rel})$, from direction ϕ_i^{rel} , the total collision probability is

$$P_T = \sum_i f(\phi_i^{rel}) A_{\otimes}(\phi_i^{rel}) = \sum_i f(\phi_i^{rel}) \int_{A=0}^{\infty} P(A) dA \quad . \quad (5.9)$$

The risk reduction, assuming a maneuver is always executed if the collision probability exceeds P_m is:

$$Q_T = \sum_i f(\phi_i^{rel}) \int_{A=0}^{A(P_m)} P(A) dA \quad . \quad (5.10)$$

The residual risk is

$$R_T = \sum_i f(\phi_i^{rel}) \int_{A(P_m)}^{\infty} P(A) dA \quad . \quad (5.11)$$

Clearly

$$P_T = Q_T + R_T \quad . \quad (5.12)$$

In the collision probability computation, the directionality of the debris is taken into account by considering angles between velocity vectors of 0° , 30° , 60° , 90° , 120° , 135° , and 150° . These correspond, approximately, to relative angles of 90° , 75° , 60° , 45° , 30° , and 15° .

The process is essentially self-verifying since

$$P_T = \sum_i f(\phi_i^{rel}) A_{\otimes}(\phi_i^{rel}) = Q_T + R_T \quad . \quad (5.13)$$

Table 5.1 shows:

- 1) The quantities defined in equations 5.8, 5.9, summed over all 15 accuracy bins as #MANEUVERS and #HITS, for an 8-hour propagation, assuming the target vehicle is tracked with the uncertainty associated with a LEO object with 22 tracks per day and an EDR of 0.005 watts/kg, using equation 1.2. The radial - down track correlation coefficient, ρ , defined by equation 5.2 was arbitrarily taken to be 0.5.
- 2) The quantities defined in 1) scaled for a 24-hour propagation.

The column designated as FRR, or fractional residual risk, represents that fraction of the no-maneuver risk that remains if a maneuver is performed for the tabulated P_m . A 60-meter radius sphere target vehicle is assumed.

Figure 5.1 shows the total collision probability versus total annual maneuver rate for 8 hours of propagation and 24 hours of propagation from epoch. The P_m values for the points are indicated on the graph. Figure 5.2 shows fractional residual risk versus annual maneuver rate.

Table 5.1 Combined maneuver rate, vehicle collision probability (#HITS) and fractional residual risk (FRR) for given P_m values

8-hour propagation				24-hour propagation			
P _m	#MANEUVER S	#HITS	FRR	P _m	#MANEUVER S	#HITS	FRR
1.460E-01	0.000E+00	5.109E-04	1.000E+00	8.860E-02	0.000E+00	5.118E-04	1.000E+00
3.000E-03	1.079E-01	1.544E-04	3.022E-01	3.000E-03	1.240E-01	2.364E-04	4.618E-01
1.000E-03	2.559E-01	1.066E-04	2.087E-01	1.000E-03	3.111E-01	1.731E-04	3.383E-01
3.000E-04	5.924E-01	6.895E-05	1.350E-01	3.000E-04	7.728E-01	1.239E-04	2.421E-01
1.000E-04	1.135E+00	4.987E-05	9.760E-02	1.000E-04	1.996E+00	8.267E-05	1.615E-01
3.000E-05	2.380E+00	3.736E-05	7.312E-02	3.000E-05	4.392E+00	5.715E-05	1.117E-01
1.000E-05	6.139E+00	2.399E-05	4.695E-02	1.000E-05	8.034E+00	4.429E-05	8.653E-02
3.000E-06	1.044E+01	1.900E-05	3.719E-02	3.000E-06	2.326E+01	2.966E-05	5.794E-02
1.000E-06	2.269E+01	1.535E-05	3.004E-02	1.000E-06	4.632E+01	2.118E-05	4.138E-02
1.070E-11	1.088E+03	0.000E+00	0.000E+00	9.380E-12	5.617E+03	0.000E+00	0.000E+00

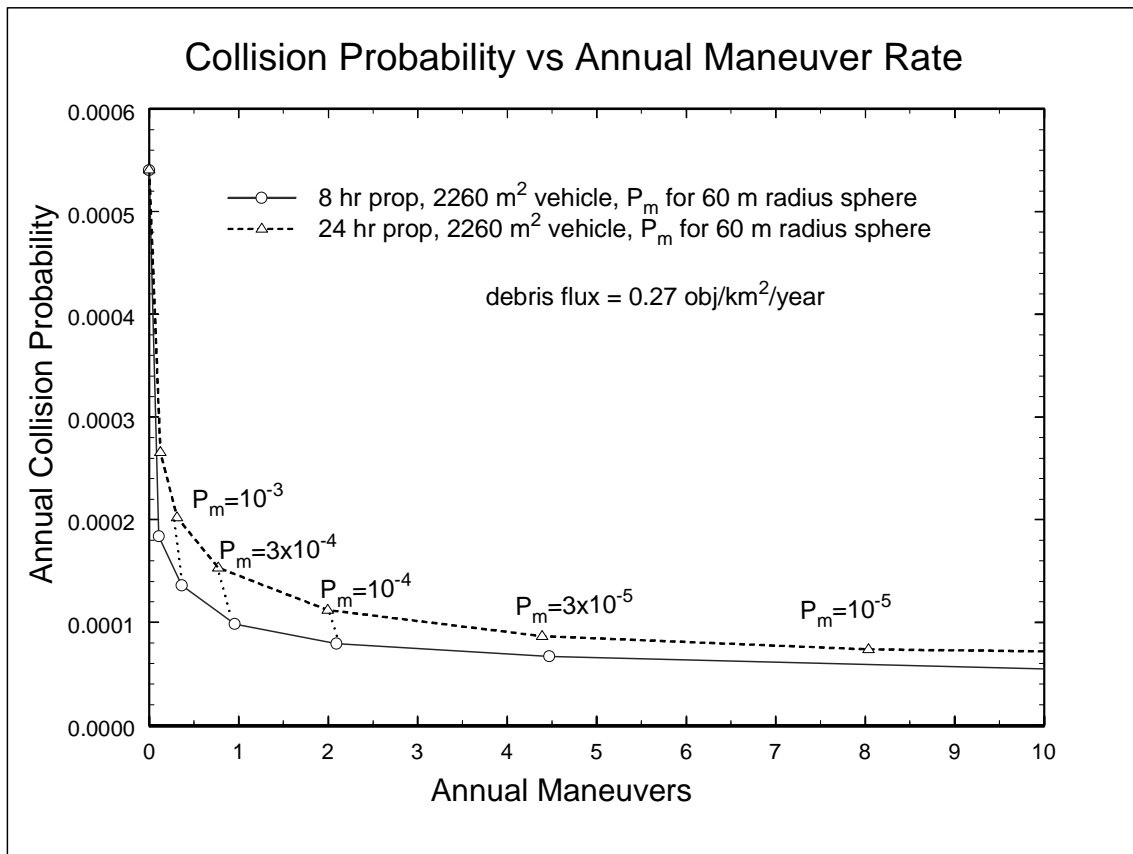


Figure 5.1 Collision probability versus annual maneuver rate for 8 and 24-hour propagation.

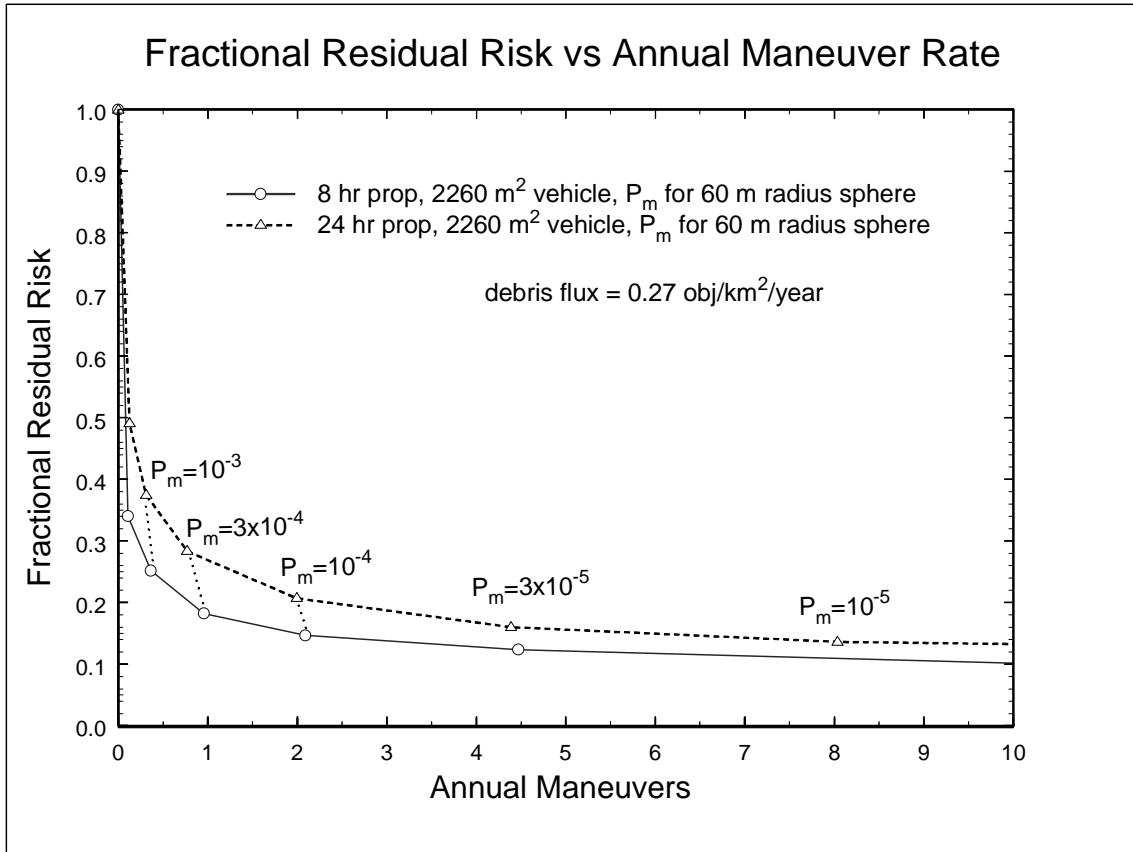


Figure 5.2. Fractional residual risk versus annual maneuver rate for 8 and 24-hour propagation.

Figures 5.1 and 5.2 indicate risk over time and maneuver rate as a function of P_m . The significance of P_m , the collision probability for which a maneuver is to be performed, requires some discussion. P_m is the collision probability with a 60-meter radius sphere with its center at the center of ISS. The ISS cross section, including solar panels, occupies only 20% of the area of the cross section of the sphere. The solar panels are over half of the ISS cross-section. Although collateral damage is possible, there is less risk to life and critical systems associated with a strike to the panels. Not taking into account the area of the solar panels reduces the collision probability by over a factor of 2. Thus the collision probability with the ISS modules and truss is an order of magnitude lower than the value for the 60-meter sphere.

We make the assumption that a maneuver eliminates the risk for the conjunction for which it was made. Still, no matter how many maneuvers are performed, risk from tracked debris is never eliminated. For values of P_m below 10^{-4} , increased maneuver rate does not result in substantial reduction in residual risk. In determining the threshold, the risk to ISS from the maneuver, the cost of the additional operational constraints due to the maneuver and the cost of loss of micro-gravity need to be taken into consideration. Further, there is a small risk of loss of vehicle associated with each maneuver; it is difficult to imagine that risk to be less than 5×10^{-7} .

2.6 Discussion

A preliminary study using a 9/7/97 (Reference 11) catalog did not include the DSP objects and did not consider the radial - down track correlation. The 11/9/98 atmospheric density is more than double that of the previous study. A much more refined regression analysis of the covariance distribution is employed in this present study.

The validity of these results depends on a maneuver being performed each and every time the collision probability for a conjunction exceeds the maneuver threshold. Performing a maneuver every time a threshold of 3×10^{-4} is exceeded, we anticipate a fractional residual risk of about 0.2 (80% risk reduction) with about 0.8 maneuvers per year. Performing a maneuver for half of the time a threshold of 10^{-5} is exceeded, results in a fractional residual risk of 0.55 (45% risk reduction) with about 4 maneuvers per year.

The maximum collision probability associated with a conjunction is about 0.1 or 10%. Prudent operations require that a contingency maneuver always be possible and that it always be performed when a sufficiently high Red Threshold collision probability is exceeded. A maneuver should be performed for a lower Yellow Threshold if the maneuver is operationally convenient.

The validity of this entire document depends on the orbit determination process being carried out with the same fit intervals and data rejection criteria used by automated program in the Kaman Sciences Study. Covariances transmitted to the MCC which vary appreciably from update to update would be an indication this is not being done. In particular the ISS MCC scaling table is based upon Equation 1.1.

Because of the high variability of the covariances produced by the SSN, 99% confidence limits (Reference 10) were established for the scaling of the workstation covariances using the software developed for the study described in Reference 3. Use of the confidence limits, while adding operational complexity, can *simultaneously reduce risk and maneuver rate* if a higher threshold is chosen. This is because the scaling increases maneuver rate and nearly eliminates risk for well-tracked objects with an intrinsically low associated maneuver rate, while not affecting the maneuver rate for poorly tracked objects for which debris avoidance is not nearly as effective.

3.0 REFERENCES

- 1) A Parametric Analysis of Orbital Debris Collision Probability and maneuver Rate for Space Vehicles, JSC-25898, August, 1992.
- 2) ISS Debris Avoidance Operations Plan, JSC DM33, in draft October 6, 1997.
- 3) Space Station Debris Avoidance Study final report, Kaman Sciences Corporation, KSPACE 97-47, January 31, 1997.
- 4) GAO Report, Space Surveillance, December 1997, GAO/NSIA-98-42
- 5) Kessler, D. J., ICARUS, 48, 39-48, Derivation of the Collision Probability of Jupiter's Moons, 1981.
- 6) Position Error Covariance Matrix Scaling Factors for Early ISS Debris Avoidance, JSC DM33, May 29, 1998.
- 7) A Computer Based Orbital Debris Environment Model for Space Craft Design and Observation in Low Earth Orbit, NASA TM 104825, November 1996.
- 8) A 160-Day Simulation of Space Station Debris Avoidance Operations with the United States Space Command (USSPACECOM), NASA/TM-2006-213720, May 2006.
- 9) Characterization of the Orbital Debris Environment Using the Haystack Radar, JSC 32213, April 24, 1992.
- 10) Effect of Covariance Confidence Limits on Maneuver Rate and Residual Risk, in draft July, 1998.
- 11) ISS Debris Avoidance Maneuver Threshold Analysis, JSC, DM33, July 6, 1998.

APPENDIX 1. COMPARISON OF FILTERED SATRAK OUTPUT TO REAL-WORLD TRACKING

We first determined the tracking opportunities for a subset of the Kaman study satellites, using SATRAK. Nineteen of those satellites classified by Kaman as the “original 20”, or well-tracked satellites were used, in addition to 15 of those classified as the “remaining satellites.” (Reference 3) Two-line element sets for these 35 satellites were obtained from USSPACECOM, with epoch times during the study period. In order to reduce error in our tracking predictions, we obtained twelve sets of the two-line elements, spaced approximately equally throughout the 108-day period of the Kaman study. SATRAK was then run in twelve segments over that period, from 1995 day 352 through 1995 day 094. The initial analysis was performed using only Low Earth Orbit (LEO) satellites for reasons discussed in the Overview, i.e., it was assumed there would be no maneuvers for deep space objects. For the Kaman study satellites, the radars were tasked for data on every pass; however, the archived sensor data were in some cases much less than simple sensor-satellite geometry would predict.

The actual SSN observations for the same 35 satellites over the 108-day period were also obtained from USSPACECOM. Sensors which contributed to these observations are those listed in Table 2.1 as “collateral support” and the “dedicated” radar at Eglin AFB.

The results of comparing actual tracking data to predicted is shown in Table A1.1. The ratio of actual to predicted tracks ranged from 30% for Kaena Point to 90% for Eglin. This ratio is defined as the duty factor.

Table A.1 Comparison of Actual Tracks to Predicted Tracks for 108-day Period

SSN Sensor Number	Total Actual Tracks	Avg. Actual Trks/Day	Total SATRAK Tracks	Avg. SATRAK Trks/Day	Actual Percent of SATRAK	SSN Sensor Name
344	9983	92.4	14294	132.352	69.8%	Fylingdales
354	8350	77.3	12654	117.167	66.0%	Ascension
359	3371	31.2	12918	119.611	26.1%	Clear, AK
363	8805	81.5	11750	108.796	74.9%	Antigua
386	8316	77.0	14192	131.407	58.6%	Cape Cod
388	9436	87.4	14219	131.657	66.4%	Beale
394	8968	83.0	12579	116.472	71.3%	Thule
396	6422	59.5	8445	78.194	76.0%	Cavalier (PARCS)
399	10601	98.2	11777	109.046	90.0%	Eglin
932	4751	44.0	15708	145.444	30.2%	Kaena Point

Because the amount of actual tracking data is less than predicted amount, we determined that a “duty factor” should be estimated for each sensor, using the Kaman study data. The duty factor, as we defined it, was the tracking performance-to-opportunities ratio averaged over the length of the study.

APPENDIX 2. RELATION BETWEEN OBJECT SIZE AND RADAR CROSS SECTION

JSC Space and Life Sciences Division carried out a study of radar cross sections for objects of different shapes, varying the wavelength from much smaller than the objects to much larger (Reference 8). Figure A1.1 shows their data result and Figure A1.2 shows their fit to the data. They broke the region of interest up into a large number of regions with a separate expression for each region. Here we produce a simplified expression using their basic result.

The expression for RCS for the MIE region was taken as an interpolation between the RCS value for Rayleigh scattering for $\frac{D}{\lambda} = 0.22$, and optical scattering for $\frac{D}{\lambda} = 1.0$, assuming an

expression of the form $RCS = \lambda^2 K \left(\frac{D}{\lambda} \right)^q$. For optical scattering at $\frac{D}{\lambda} = 1.0$,

$$RCS = \lambda^2 \frac{\pi}{4} (1)^2 = \lambda^2 K (1)^q \quad \text{implies that } K = \frac{\pi}{4} = 0.7853982 \quad .$$

For Rayleigh scattering at $\frac{D}{\lambda} = 0.22$,

$$RCS = \lambda^2 \left(\frac{9\pi^5}{4} \right) (0.22)^6 = \lambda^2 \frac{\pi}{4} (0.22)^q \quad \Rightarrow \quad q = \frac{\log_{10} \left(\frac{4}{\pi} \frac{9\pi^5}{4} (0.22)^6 \right)}{\log_{10}(0.22)} = 1.524721 \quad .$$

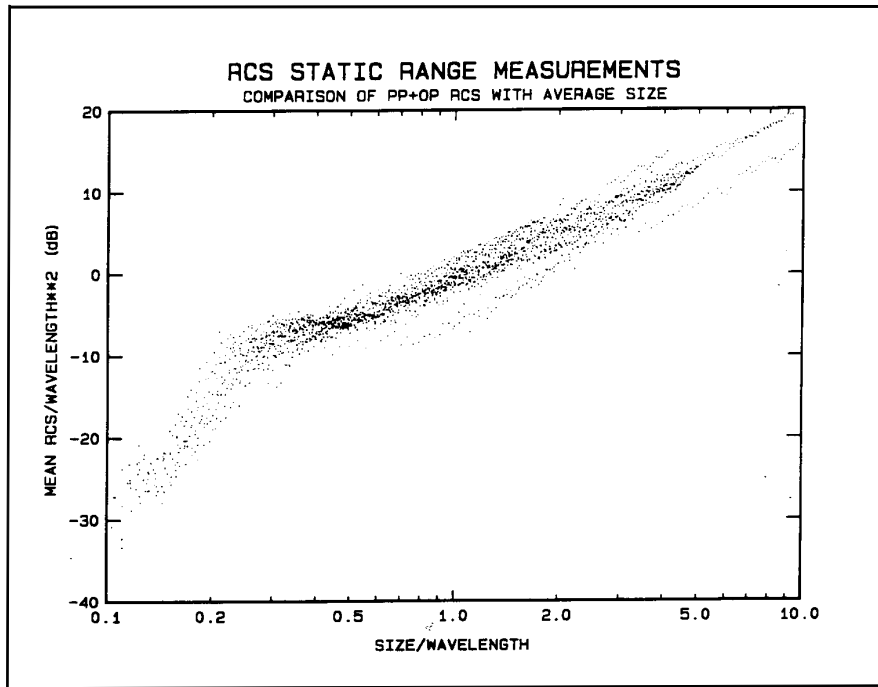


Figure A.1 Experimental mean RCS to wavelength data from Reference 8.

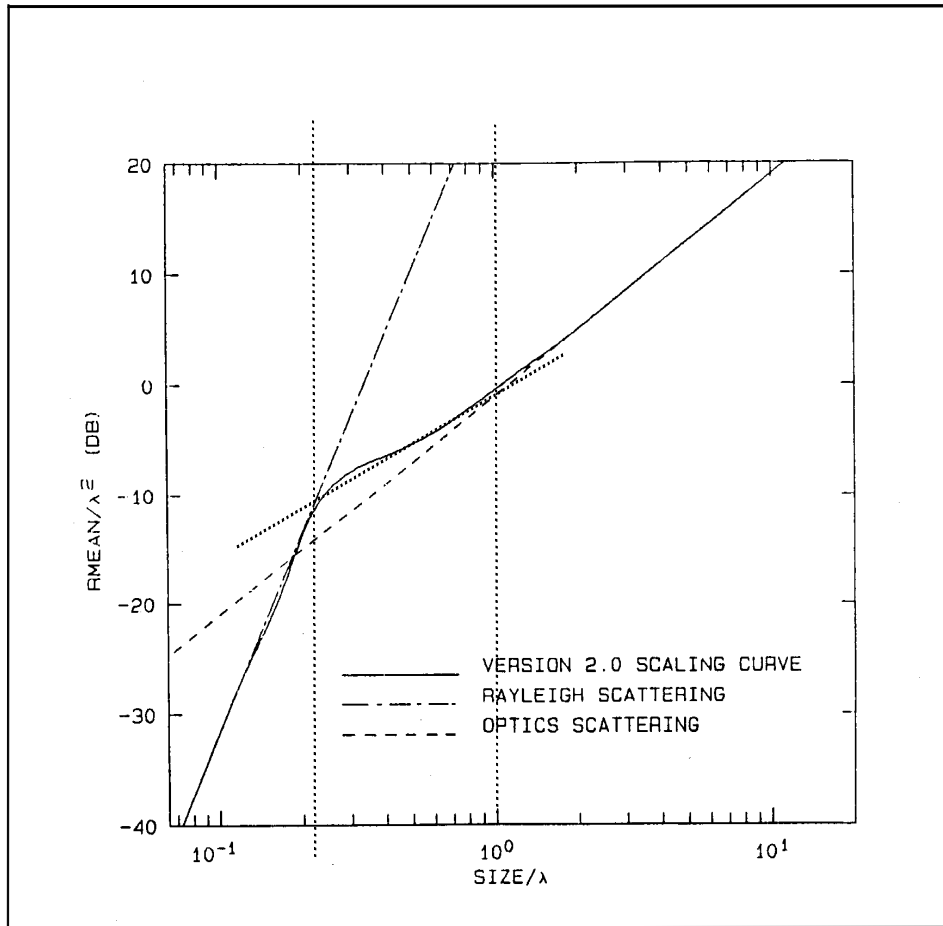


Figure A.2 Fit from Reference 8 is indicated by solid curve and fit for this work to the region between $\lambda/D=1$ and $\lambda/D=22$, is shown by the dotted line. In this work, for values $\lambda/D>1$, the optical expression is used, and for values $\lambda/D<0.22$ the Rayleigh expression is used. The 2 vertical dotted lines indicate $\lambda/D=1$ and $\lambda/D<0.22$.

APPENDIX 3. DERIVATION OF EDR AS A FUNCTION OF TIME DERIVATIVE OF MEAN MOTION

The energy of an Earth orbiting object, E , in terms of its semi-major axis, a , is $E = -\mu_e/2a$, where μ_e is the product of the gravitational constant and the mass of the Earth. The time derivative of E is $\dot{E} = \left(\mu_e/2a^2\right)\dot{a}$. Equation 4.18 expresses the mean motion, n_0 , in terms of the semi-major axis: $n_0 = \sqrt{\mu_e/a^3}$. Solving for a , $a = \sqrt[3]{\mu_e/n_0^2}$. The time derivative of a is then

$$\begin{aligned}\dot{a} &= -2/3 \mu_e^{-1/3} n_0^{-5/3} \dot{n}_0 \\ &= -2/3 \mu_e^{-1/3} \left(\sqrt{\mu_e/a^3}\right)^{-5/3} \dot{n}_0 \\ &= -2/3 \mu_e^{-1/2} a^{5/2} \dot{n}_0\end{aligned}$$

and

$$\begin{aligned}\dot{E} &= -2/3 \left(\mu_e/2a^2\right) \mu_e^{-1/2} a^{5/2} \dot{n}_0 \\ &= -1/3 \mu_e^{1/2} a^{1/2} \dot{n}_0 \\ &= -2/3 \mu_e^{1/2} a^{1/2} \left(\dot{n}_{SPACECOM}/2\right)\end{aligned}$$

**APPENDIX 4. FLUX, EDR AND TRACKS PER DAY FOR 11/9/98
TRACKED LEO OBJECTS**

objid	Flux obj/km ²	EDR watts/sec	tracks/day	objid	Flux obj/km ²	EDR watts/sec	tracks/day	objid	Flux obj/km ²	EDR watts/sec	tracks/day
60	0.000601	0.003271	20.55	19173	0.000556	0.073432	14.6	25033	7.37E-05	0.110804	1.45
388	0.006211	0.025092	29.5	19560	0.000138	0.231693	4.55	25065	0.002206	0.047936	17.45
614	0.000325	0.004854	34.15	19771	0.000116	0.352382	16.15	25076	0.000252	0.028935	10.9
746	0.000141	0.000337	15.15	19822	8.84E-05	0.015558	19.3	25088	0.004494	0.001772	26.55
750	0.000227	0.006094	8.9	19824	0.000109	0.033396	19.8	25099	6.36E-05	0.149785	0.3
829	0.000154	0.000446	10.7	19963	0.000132	0.031441	15.3	25120	0.001312	0.085599	19.2
831	0.000249	0.0099	15.55	19993	0.000344	0.006241	3.65	25121	0.000767	0.007493	19.95
963	6.37E-05	0.021668	5.65	20021	0.000165	0.033544	9.15	25125	0.006092	0.034569	27.65
1613	0.000648	0.00134	17.3	20047	0.006134	0.019743	3.05	25137	0.000474	0.021248	17.05
1616	0.000681	0.003509	22.5	20307	0.000444	0.009855	21.8	25139	0.000508	0.060667	14.7
1844	0.004489	0.008294	26.85	20496	0.002651	0.006372	19.6	25166	0.000404	0.077148	27.2
1937	0.00218	0.005486	24.7	20774	0.000545	0.001239	31.45	25176	0.000217	0.049945	28.45
2150	0.000261	0.003591	24.65	20775	0.000652	0.003863	40.7	25251	0.002237	0.65909	13.55
2167	0.000403	0.025436	34.2	20919	0.000845	0.01236	20	25310	0.000378	0.019992	21.75
2208	0.000363	0.008445	15.55	20966	0.005151	0.007336	29.2	25347	0.001146	0.034213	27.05
2389	0.000348	0.006055	30.9	21083	0.000567	0.041161	13.45	25389	0.001061	0.003765	27.15
2800	0.000267	0.001524	19.55	21150	0.000637	0.003231	21.35	25390	0.001093	0.00722	27.05
2988	0.002949	0.075634	8.8	21393	0.000334	0.001646	27.6	25391	0.00098	0.001958	29.35
3019	0.000549	0.002271	30.9	21819	9.65E-05	0.000572	40.45	25392	0.001075	0.005893	26.5
3381	0.003858	0.059199	11.45	21820	0.000104	0.000239	37.9	25393	0.00112	0.0124	26.35
3508	0.00316	0.117062	24.4	21826	0.000147	0.008616	15.7	25421	0.000713	0.102501	15.85
3564	0.001312	0.057332	19.8	21827	0.00019	0.006865	12.8	25422	0.000956	0.008584	18.85
4053	0.000146	0.008094	15.6	21835	8.84E-05	0.0007	31.7	25472	0.001547	0.037286	25.5
4120	0.005116	0.019065	26.75	21961	0.000145	0.007197	27	25497	8E-05	0.10812	6.9
4221	0.000768	0.005431	29.3	22016	5.9E-05	0.151443	10.7	25498	9.62E-05	0.025689	4.95
4222	0.001063	0.032881	34.45	22196	0.000114	0.00855	13.5	25532	0.001028	0.100572	29.05
4330	0.000248	0.016442	13.8	22233	5.27E-05	0.048478	7.35	81019	0.000203	0.017635	13.6
4382	0.000173	0.000413	35.15	22277	4.61E-05	0.035899	8.35	81510	0.000174	0.070916	18.3
4392	0.000801	0.007718	38.7	22365	0.000798	0.017705	25	81511	8.51E-05	2.012522	10.2
4584	0.000633	0.004638	31.5	22386	0.00054	0.019034	24.55	81512	0.000265	0.684957	22.5
5093	0.000435	0.020039	17	22448	4.55E-05	0.027141	3.3	81514	5.69E-05	0.086203	4.2
5281	0.000788	0.005661	41.25	22528	0.000124	3.115348	28.6	81532	5.47E-05	0.387614	6.05
5282	0.000782	0.006003	29	22535	0.000123	0.016599	2.05	81535	0.000376	0.004448	26.4
5714	0.001119	0.01453	16.8	22564	0.000105	0.1139	24.45	81536	0.000284	0.836124	21.8
5729	0.000499	0.003332	37.7	22583	0.000559	0.038571	16.7	81552	0.000216	0.027339	14.95
5730	0.000532	0.002322	43.2	22584	9.8E-05	0.468184	17.9	81561	0.000274	0.020772	22.15
5761	0.00092	0.016067	27.2	22659	4.8E-05	0.090743	8.95	81564	0.000229	3.056946	27.15
5999	0.00019	0.00947	6.15	22702	5.58E-05	0.129768	9.55	81574	0.000119	2.243678	21.55
6073	9.72E-05	0.005383	6.75	22788	5.39E-05	0.01612	11.35	81581	0.000134	0.718327	14.75
7003	0.000669	0.002324	40.45	22845	0.000238	0.007687	19.05	81583	0.000151	1.426794	21
7004	0.000734	0.00254	30.35	22875	0.000391	0.009514	30.3	81584	0.000279	1.201699	20
7337	0.000694	0.001685	42.5	22876	0.000466	0.022212	42.35	81585	0.000187	0.650431	22.55
7338	0.000847	0.002952	29.85	22878	0.002432	0.01496	19.3	81586	0.000134	0.100709	10.6
7418	0.004017	0.026041	25.5	22879	4.74E-05	0.04362	4.15	81790	4.23E-05	18.09555	5
7969	0.005094	0.009767	28.6	22896	0.000556	0.046045	28.4	81791	7.17E-05	1E-08	5.95
8063	0.000295	0.009935	43	22922	0.000258	0.01122	25.65	81792	4.43E-05	0.001625	5.1
8133	0.000556	0.00602	24.1	22928	5.3E-05	1.711777	14.55	87076	0.00019	0.089148	19.5
8368	0.000377	0.322802	16.9	23029	4.49E-05	0.069398	3.6	87090	0.002486	0.04594	25.65
8702	0.00013	0.067612	16.05	23099	0.000859	0.003082	21.05	87124	0.00019	0.05812	20.25
8744	0.000676	0.001871	40.05	23100	0.000354	0.002547	20.7	87137	0.000177	0.079701	18.95
8745	0.000987	0.004645	39.65	23186	4.34E-05	0.287921	5.8	87138	0.000578	0.009278	22.5
8755	0.005125	0.022432	26.7	23191	0.000445	0.003995	44.95	87147	0.000205	0.068839	18.95
8940	0.006181	0.034502	23.15	23198	0.000473	0.003027	35.15	87170	0.000203	0.130389	19.85
9854	0.003959	0.007682	29.1	23278	0.000491	0.000988	34.35	87246	0.000264	0.088669	12.8
9974	0.002031	0.115728	16.7	23279	0.000548	0.001903	31.25	87284	0.000217	0.448514	32.6

objid	Flux obj/km ²	EDR watts/sec	tracks/day	objid	Flux obj/km ²	EDR watts/sec	tracks/day	objid	Flux obj/km ²	EDR watts/sec	tracks/day
10135	0.002118	0.006273	28.95	23281	0.000773	0.022835	31.3	87288	0.000125	0.049818	4.55
10223	0.000897	0.017467	23.1	23295	0.000125	0.146641	13.05	87297	0.000137	0.089197	15.55
10269	0.000728	0.008318	6	23316	7.66E-05	1.804282	15.15	87345	0.001226	0.01471	27.7
10634	0.000115	0.004305	5.15	23502	0.000646	0.007016	29.45	87361	0.000258	0.000642	27
11221	0.000758	0.007997	25.05	23529	4.83E-05	0.759542	12.1	87363	0.000187	0.018265	20.35
11240	4.71E-05	2.956717	9.85	23539	3.52E-05	1.22608	7.25	87364	7.34E-05	0.523727	4.1
11765	0.000675	0.001385	32.8	23563	9.15E-05	0.138868	8.85	87387	0.000235	0.046713	16.2
11781	0.000689	0.003013	19.15	23769	0.000538	0.0044	27.3	87396	0.000146	0.062821	15.25
12069	8.19E-05	0.017211	14.9	23834	0.000516	0.008016	20.15	87400	0.00039	0.020091	32.25
12138	0.000553	0.001395	44.85	23853	0.000383	0.006234	41.05	87455	6.63E-05	0.002773	2.75
12139	0.000637	0.003115	46.1	23854	0.000393	0.016507	43.15	87496	0.000143	0.09014	19.5
12354	0.000514	0.001126	25.25	23878	0.000368	0.008956	26.15	87542	7.54E-05	0.066887	9.85
12388	0.000632	0.001659	30.45	23941	0.000943	0.013192	32.15	87618	0.000535	0.015479	25.95
12389	0.000803	0.00357	42.7	23980	0.000399	0.071646	24.5	87623	6.32E-05	0.223125	6.1
12497	7.37E-05	0.005813	10	23995	0.000312	0.014675	26.4	87626	0.000109	0.09381	19.05
12519	4.84E-05	0.417899	4.05	24008	0.000574	0.194404	22.8	87627	0.000162	0.615541	22.9
12848	0.000591	0.002099	32.8	24087	0.001927	1.449741	5.1	87641	4.83E-05	0.084998	4.35
12849	0.000498	0.000433	32.2	24142	0.004049	2.956212	1.1	87651	0.000291	0.138987	17.95
12908	7.18E-05	0.025173	12.9	24237	0.002616	0.245948	23.25	87657	0.000144	0.03209	12.35
13007	6.33E-05	0.005616	5.85	24264	0.001129	0.238034	26.65	87719	0.004538	0.09104	28.1
13985	0.000228	0.018162	22.9	24285	0.000288	0.003139	27.05	87773	0.000516	0.00897	26.3
14051	0.000304	0.00253	22.55	24286	0.000278	0.00337	27.5	87778	5.75E-05	0.088015	4.1
14168	8.81E-05	0.217998	13.65	24291	0.000654	0.019085	30.4	87799	0.000133	0.088689	9.8
14236	7.34E-05	0.045478	8.35	24317	0.00028	0.017163	17.8	87806	0.000422	0.013216	28.75
14329	0.000383	0.055247	19.1	24319	0.00034	0.100662	17.15	87807	0.000152	0.120327	13.85
14483	0.000571	0.001569	43.5	24325	0.000345	0.09892	10.6	87809	0.000115	1E-08	6.4
14484	0.000796	0.003959	38.7	24430	0.002826	0.043164	16.2	87810	0.000154	2.477307	23.95
14693	0.000569	0.008754	16.5	24520	0.002326	0.456355	16.15	87815	0.000225	0.083117	18.25
14694	0.000404	0.003031	22.85	24565	0.000754	0.070237	21.35	87818	9.78E-05	1.976704	20.85
15076	6.8E-05	0.21088	10.1	24646	0.000384	0.019738	22.55	87820	0.00017	0.004315	27.35
16084	0.006155	0.007412	26.95	24670	0.004495	0.00264	26.65	87821	5.3E-05	0.377755	6.2
16308	0.006178	0.011892	24.8	24698	0.005141	0.677302	27.65	87830	9.23E-05	0.379799	8.7
16311	0.006142	0.003906	27.9	24744	0.0024	0.013524	29.55	87832	0.000223	0.266919	22
16480	0.006145	0.004423	26.05	24831	0.00067	0.023386	11.85	87835	5.12E-05	0.622341	8.3
16545	0.00042	0.025785	16.7	24832	0.000245	0.072991	24.45	87838	7.39E-05	0.0945	5.25
16547	0.000565	0.018568	6.05	24972	0.000919	0.0243	25.95	88011	7.31E-05	0.261668	17.6
16609	0.001464	0.015735	21.3	24995	0.000667	0.016778	33.65	88017	7.98E-05	0.279288	2.7
16878	0.000577	0.003296	19.15	25013	0.001249	0.004146	20.4	88380	0.000132	0.590179	24.95
17094	0.002453	0.003199	27.65	25014	0.00192	0.011757	20.1	88520	0.000134	0.342804	23.3
18872	0.001962	0.167759	17.5	25018	0.000774	0.003895	27.15	88856	5.58E-05	0.110845	23.35

**APPENDIX 5. FLUX, EDR AND TRACKS PER DAY FOR 11/9/98
TRACKED DSP OBJECTS**

objid	Flux obj/km ²	EDR watts/sec	tracks/day	objid	Flux obj/km ²	EDR watts/sec	tracks/day	objid	Flux obj/km ²	EDR watts/sec	tracks/day
2643	3.83E-05	0.001358	7.05	20474	1.7E-05	0.001611	6	24878	3.29E-05	0.158568	10.65
4298	3.85E-05	0.001074	6.05	20559	2.09E-05	0.00312	7.45	24892	1.3E-05	0.016784	6.4
4354	2.33E-05	0.002571	6.15	20630	6.78E-05	0.000459	11.5	24934	2.21E-05	0.065383	11.55
5975	2.53E-05	0.001123	7.15	20631	3.18E-05	0.000371	11.85	24937	1.2E-05	0.005645	6.5
5977	2.61E-05	0.0025	7.65	20669	1.66E-05	0.000923	5.95	24990	5.59E-05	0.003436	10.45
5998	3.16E-05	0.014529	9.4	20698	2.1E-05	0.067143	7.25	25032	3.17E-05	0.088257	14.5
7794	3E-05	0.007307	10.2	20704	3.18E-05	0.137495	16.2	25053	1.6E-05	0.005279	4.4
8134	3.47E-05	0.000351	4.6	20712	2.6E-05	0.000747	6.7	25054	2.33E-05	0.047881	7.05
8546	7.1E-05	0.000501	8.95	20713	2.25E-05	0.001568	7.05	25069	1.44E-05	0.091259	7.45
8910	2.57E-05	0.002832	9.3	20717	2.25E-05	0.000176	5.55	25070	1.46E-05	0.06065	7.4
9017	4.41E-05	0.010532	15.2	20718	2.01E-05	0.013589	7.15	25090	2.84E-05	0.016149	13.65
9330	3.07E-05	0.000702	7.45	20764	2.11E-05	5.64E-05	4.9	25098	2.28E-05	0.002423	8.9
9850	1.29E-05	0.002488	4.85	20843	1.97E-05	0.001589	5.85	25111	1.25E-05	0.040332	6.85
9864	3.6E-05	0.005139	11.35	20874	1.63E-05	0.010573	6.95	25129	1.7E-05	0.109752	4.05
9927	1.36E-05	0.001038	5.45	20947	1.74E-05	0.004704	8.35	25151	3.38E-05	0.007256	11.15
9980	1.37E-05	0.009351	6.8	21012	3.05E-05	8.78E-05	7.85	25154	1.23E-05	0.058108	6.5
10155	3.13E-05	0.000162	6.25	21013	4.28E-05	0.003418	8.35	25155	1.31E-05	0.091356	6.95
10723	2.05E-05	0.005568	8.5	21025	3.19E-05	0.064785	13.5	25240	1.45E-05	0.118631	7.55
10960	4.58E-05	0.004479	10.15	21114	3.36E-05	0.010962	12.5	25259	2.18E-05	0.037034	8.25
10983	2.74E-05	0.006241	7.9	21141	2.56E-05	0.010979	8.5	25279	3.56E-05	0.000987	7
11007	2.63E-05	0.000161	7	21151	2.1E-05	0.033719	11.25	25313	1.16E-05	0.028005	8.1
11027	2.78E-05	0.004875	10.5	21538	2.82E-05	0.233562	9.75	25314	1.3E-05	0.063265	8.4
11028	3.87E-05	0.003347	10.6	21588	3.91E-05	0.000549	4.1	25355	3.91E-06	0.100336	4.7
11474	2.44E-05	0.000201	5.3	21589	2.63E-05	0.000548	4.25	25372	1.31E-05	0.008525	6.4
11553	1.25E-05	0.00321	4.85	21634	2E-05	0.001252	4.65	25461	1.62E-05	0.001204	6.05
11718	3.86E-05	0.003404	10.1	21635	2.02E-05	0.001534	4.65	25493	1.2E-05	0.018075	5.8
12133	1.36E-05	0.002758	4.8	21637	3.98E-05	0.000275	4.4	25494	1.34E-05	0.029703	1.85
12134	1.56E-05	6.1E-05	5.65	21640	2.01E-05	0.000955	6.45	25496	1.2E-05	0.06584	4.95
12295	3.48E-05	0.007262	9.4	21654	1.64E-05	0.010456	5.65	25499	1.46E-05	0.409342	5.8
12445	0.000112	0.002455	20.4	21727	2.44E-05	0.000317	7.65	25500	1.4E-05	0.018732	4.6
12546	2.16E-05	0.000869	7.25	21766	1.56E-05	0.00961	5	25502	2.37E-05	0.003612	7.55
12787	2.07E-05	0.001977	7.4	21778	2.84E-05	0.000778	3.7	25517	1.2E-05	1E-08	4.8
13011	1.8E-05	0.001272	7.45	21815	1.95E-05	0.000119	6.9	25518	1.23E-05	0.076465	5.4
13070	9.32E-06	9.53E-05	7.3	21818	2.34E-05	0.00259	5.15	80480	7.31E-05	0.012175	11.05
13075	3.3E-05	8.36E-05	5.6	21829	3.77E-05	0.069285	16.7	80503	4.95E-05	0.035179	11.15
13608	5.59E-05	0.006256	17.75	21941	1.67E-05	0.004277	8.25	81073	7.51E-05	0.005044	6.55
13609	5.01E-05	0.00807	10.05	21942	2.42E-05	0.002199	7.1	81102	7.55E-05	0.008329	8.6
13658	2.04E-05	0.002797	6.45	21960	9.17E-05	0.325555	14.9	81105	5.07E-05	0.007245	13.05
13666	2.04E-05	0.001829	6.4	21990	2.14E-05	0.012046	7.5	81107	4.16E-05	0.010723	15.2
13904	2.8E-05	0.004856	10.7	22032	1.67E-05	0.009805	7.15	87834	5.75E-05	0.758906	12.4
13908	4.39E-05	0.000366	6.15	22033	2.9E-05	0.018277	9.65	88001	5.98E-05	0.00179	9.15
13909	4.82E-05	0.000641	6.1	22048	2.07E-05	0.184308	7.35	88008	6.8E-05	0.00228	9.8
13910	3.26E-05	0.006323	9.1	22089	2.95E-06	1E-08	6	88050	4.2E-05	0.000667	7
13911	2.75E-05	0.033957	14.3	22250	2.73E-05	0.036562	13.8	88062	7.33E-05	0.00261	10.05
13912	3E-05	0.002466	9.25	22254	1.52E-05	0.013219	7.9	88064	9.42E-05	0.006953	10.1
13958	2.5E-05	0.002901	7.15	22274	2.2E-05	0.003874	6.65	88079	9.81E-05	0.004096	13.55
13967	2.11E-05	4.58E-05	5.9	22315	1.68E-05	0.00221	6	88107	3.02E-05	0.006275	6.45
13971	1.95E-05	0.00538	6.2	22655	1.98E-05	0.000706	6.55	88113	3.83E-05	0.003105	7.4
14135	2.02E-05	0.000495	6	22656	2.03E-05	0.006044	6.9	88126	4.07E-05	0.030091	12.5
14136	1.98E-05	0.00127	8.8	22670	2.64E-05	0.000683	10.4	88143	5E-05	0.006699	8.5
14277	9.1E-05	0.00025	8.6	22725	2.25E-05	0.000615	6.75	88150	5.57E-05	0.00148	7.35
14278	9.26E-05	0.000505	7.55	22726	2.56E-05	0.064337	8.6	88155	2.32E-05	0.005604	6.1
14524	2.14E-05	0.001564	6.9	22781	3.95E-05	0.042002	20.9	88162	5.7E-05	0.001101	7.75
14607	0.000109	0.001284	9.25	22797	1.78E-05	0.000875	6.75	88164	4.17E-05	0.021012	12.2
14608	9.02E-05	0.001305	8.15	22851	1.65E-05	0.053569	7.55	88177	2.28E-05	0.000951	6.05

objid	Flux obj/km ²	EDR watts/sec	tracks/day	objid	Flux obj/km ²	EDR watts/sec	tracks/day	objid	Flux obj/km ²	EDR watts/sec	tracks/day
14756	3.07E-05	0.005042	6.3	22913	2.23E-05	0.073889	8.4	88178	4.14E-05	0.003338	8.25
14900	1.82E-05	2.09E-05	6.6	22925	2.52E-05	0.008484	11.9	88180	5.36E-05	0.00789	11.7
15053	5.43E-05	0.001712	9.05	22933	3.27E-05	0.006752	9.2	88189	3.84E-05	0.01183	10.85
15054	6.11E-05	0.002946	9.2	22968	2.55E-05	0.019175	11.25	88199	6.6E-05	0.016015	13.45
15188	1.63E-05	0.000129	5.75	22979	2.65E-05	2E-05	6.75	88207	1.91E-05	0.00127	6.2
15244	5.24E-05	0.005088	17.05	22980	2.3E-05	0.000795	5.15	88210	2.16E-05	0.000576	6.2
15245	2.74E-05	6.96E-05	6.5	22986	2.59E-05	0.093952	8.95	88212	6.46E-05	0.010663	11.7
15246	2.72E-05	0.000964	8.6	22996	1.41E-05	0.004084	6.85	88215	4.05E-05	0.003386	11.8
15265	7.13E-05	0.000873	9	22997	1.92E-05	0.057108	9.15	88251	6.4E-05	0.002562	13
15266	7.77E-05	0.000949	10.55	23009	2.13E-05	0.020465	10.45	88257	1.71E-05	0.031819	7.25
15387	4E-05	0.000178	6.5	23049	4.02E-05	0.002047	11.5	88260	1.04E-05	0.001112	5.05
15388	3.98E-05	0.000477	6.55	23050	3.74E-05	0.003174	11.5	88273	5.6E-05	0.001723	9.5
15390	6.42E-05	0.003165	14.45	23117	2.44E-05	0.010987	9.65	88281	1.55E-05	0.008049	4.8
15562	2.25E-05	0.000757	6.45	23125	1.44E-05	0.001712	4.5	88337	3.75E-05	0.09694	6.85
15644	2.27E-05	0.000788	8.35	23126	1.48E-05	0.001662	5	88338	9.09E-05	0.000942	12.65
15679	2.28E-05	0.021089	7.55	23127	2.14E-05	0.000429	6.3	88340	6.72E-05	0.003952	10.55
15714	5.95E-05	0.001656	11.65	23133	4.07E-05	0.027818	14.25	88346	5.38E-05	1E-08	8.75
15715	4.76E-05	0.006955	12.4	23172	3.43E-05	0.101846	10.95	88347	3.14E-05	0.002371	4.9
15832	2.62E-05	1.38E-05	5.75	23174	2E-05	0.003364	4.5	88354	1.6E-05	0.021853	4.7
15836	2.08E-05	9.11E-05	5.85	23177	2.5E-05	9.05E-05	6.7	88355	4.07E-05	0.000417	11.95
15837	2.48E-05	0.000105	6.3	23178	2.19E-05	0.011201	7.5	88357	5.28E-05	0.009687	10.1
15874	2.07E-05	0.001487	6.25	23201	3.48E-05	0.000309	7.25	88358	3.05E-05	0.00851	8.85
15876	3.73E-05	0.000916	6.8	23209	4.02E-05	0.003445	11.95	88386	1.71E-05	0.000199	5.4
15916	2.5E-05	1E-08	5.45	23210	4.31E-05	0.002571	11.95	88388	1.75E-05	0.019837	5.3
15957	3.2E-05	0.035203	13.9	23229	1.23E-05	0.000162	6.75	88391	3.11E-05	0.003946	5.95
15977	1.36E-05	0.052759	7	23232	2.25E-05	0.092622	9.2	88402	0.000102	0.005985	10.7
15983	1.21E-05	0.125799	6.7	23236	1.93E-05	0.037121	8.55	88410	2.57E-05	0.00777	5.9
15996	3.12E-05	6.46E-05	5.1	23246	2.39E-05	0.013246	9.65	88415	2.36E-05	0.045949	8.95
16001	8.92E-05	0.000621	12.05	23249	1.65E-05	0.049797	6.3	88423	1.02E-05	0.00016	5.85
16007	3.32E-05	0.000265	5.1	23332	1.66E-05	0.016873	5.85	88425	2.25E-05	0.002102	6.2
16102	2.17E-05	0.004668	8.45	23416	1.87E-05	0.073956	11.9	88431	3.29E-05	0.006559	3.45
16187	1.21E-05	0.011958	4.35	23430	1.94E-05	0.237042	7.15	88435	2.8E-05	0.064721	13.85
16220	3.95E-05	0.00036	8.3	23460	1.58E-05	0.030676	5	88451	0.000132	0.023844	12.6
16229	6.22E-05	0.002371	16.15	23468	2.33E-05	0.004202	10.55	88459	6.03E-05	0.016497	15.05
16293	3.13E-05	7.64E-05	6.95	23517	3.11E-05	0.000204	9.75	88461	3.23E-05	0.010632	10.35
16294	2.96E-05	0.000129	6.4	23518	5.79E-05	8.82E-05	9.65	88490	4.14E-05	0.084674	17.1
16295	3.58E-05	0.000286	7.85	23523	2.11E-05	0.001394	7	88497	3.57E-05	0.000892	10
16483	2.76E-05	0.000185	7	23538	1.94E-05	0.001047	6.5	88505	2.63E-05	0.012479	8.4
16600	4.11E-05	0.047145	14.65	23554	1.73E-05	0.027166	7.1	88516	1.01E-05	0.001419	2.7
16657	1.53E-05	5.47E-05	5.75	23590	2.47E-05	0.006726	10.8	88518	1.85E-05	0.023411	6.05
16683	1.22E-05	0.020096	6.35	23599	1.77E-05	0.003375	6.9	88536	4.63E-05	0.006689	10.1
16686	1.43E-05	0.001109	6.55	23614	1.69E-05	0.002672	7.55	88537	8.95E-05	0.003299	10.35
16885	3.36E-05	0.001039	7.15	23630	5.5E-05	0.000228	10.55	88541	2.58E-05	0.007175	7.3
17038	1.94E-05	0.001476	7.45	23631	6.85E-05	0.000229	10.7	88544	0.00011	0.010532	10.5
17041	1.42E-05	0.002637	6.3	23661	2.26E-05	0.117564	7.6	88548	4.59E-05	0.00211	7.4
17325	2.41E-05	0.000754	6.8	23671	3.48E-05	0.000303	5.25	88553	2.76E-05	0.002456	6.05
17563	1.92E-05	0.001658	6.95	23697	2.27E-05	0.004593	8.05	88564	7.31E-05	0.003248	9.5
18332	2.53E-05	0.011987	8.15	23725	1.6E-05	0.003287	5.95	88566	2.61E-05	0.002948	8.3
18374	4.03E-05	0.000458	10.5	23732	1.59E-05	0.001129	6.3	88569	1.02E-05	0.000765	7.15
18375	7.92E-05	0.000593	12.25	23733	1.86E-05	0.103274	8.7	88570	5.39E-05	0.00067	7.8
18571	2.31E-05	0.001389	7.15	23742	1.74E-05	0.077869	6.9	88578	3.16E-05	0.000369	4.15
18719	3E-05	0.049069	12.15	23756	1.67E-05	0.002021	5.1	88580	2.74E-05	0.095363	11.6
18953	3.69E-05	0.000877	6.85	23766	1.56E-05	0.00114	6.45	88588	9.02E-05	0.252698	11.65
19170	4.1E-06	0.00019	6.7	23767	1.72E-05	0.149194	7.9	88596	4.69E-05	0.007935	10.9
19219	1.6E-05	0.003239	8.45	23782	1.87E-05	0.038483	7.25	88598	3.59E-05	0.003375	7.45
19220	3.26E-05	0.022286	9	23813	2.79E-05	0.000989	7.25	88599	3.3E-05	0.001179	4.85
19332	2.54E-05	0.01397	7.65	23817	1.81E-05	0.080897	7	88622	2.8E-05	0.001009	5.4
19348	3.18E-05	0.021622	12.4	23835	3.36E-05	0.048392	14.35	88625	1.46E-05	1.77E-05	4.75

objid	Flux obj/km ²	EDR watts/sec	tracks/day	objid	Flux obj/km ²	EDR watts/sec	tracks/day	objid	Flux obj/km ²	EDR watts/sec	tracks/day
19377	1.53E-05	0.230884	8.2	23847	1.56E-05	0.006483	7.2	88627	7.55E-05	0.008573	11.95
19485	2.65E-05	0.022577	10.8	23866	1.6E-05	0.004099	6.35	88630	6.01E-05	0.010722	7.45
19535	4.15E-05	0.002194	9.2	23867	1.97E-05	0.004351	6.7	88633	3.26E-05	0.005896	10.25
19537	3.76E-05	0.003654	9.6	23887	4.13E-05	0.157443	15.2	88634	2.09E-05	0.001594	9.6
19549	2.32E-05	0.00027	7.1	23944	9.93E-06	0.021558	4.6	88637	4.42E-05	0.00357	6.2
19595	4.57E-05	0.000368	3.75	23950	1.56E-05	0.004499	6.4	88638	3.47E-05	0.008186	6.35
19622	2.14E-05	0.001048	6.9	23951	1.86E-05	0.012434	6.8	88651	1.56E-05	0.012046	6.05
19733	1.45E-05	0.004355	6.3	23955	3.23E-05	0.079112	11.85	88661	4.85E-05	0.001964	8.15
19884	1.79E-05	0.012285	7.75	23966	4.34E-05	0.001509	6.95	88665	0.000115	0.278877	12.8
19920	7.71E-05	0.001391	12.05	23968	3.42E-05	0.001431	5.95	88668	7.33E-05	0.314019	11.05
19970	2.62E-05	0.005772	8.7	24211	2.03E-05	0.024223	7.05	88669	6.67E-05	0.032357	11.45
20052	1.57E-05	0.002623	6.55	24283	3.37E-05	0.008083	10.15	88671	5.97E-05	0.049859	9.05
20055	1.29E-05	0.00477	5.3	24314	1.73E-05	0.018699	6.45	88674	3.5E-05	0.245591	11.15
20081	5.26E-05	0.000732	8.2	24321	3.3E-05	0.112897	10	88676	2.98E-05	0.013507	11
20082	4.34E-05	0.001646	7.3	24654	3.51E-05	0.00035	6.6	88679	9.93E-05	1E-08	11.9
20094	2.59E-05	0.049933	8.3	24655	1.73E-05	0.009216	6.6	88683	1.99E-05	0.067018	5.25
20127	1.9E-05	0.000203	7.5	24715	1.55E-05	0.002897	6.25	88685	4.82E-05	0.133404	9.4
20170	3.4E-05	0.000824	6.4	24716	1.77E-05	0.095653	6.75	88686	7.81E-05	0.023873	8.35
20229	1.17E-05	3.88E-06	6.85	24721	2.65E-05	0.035775	9.25	88715	3.96E-05	0.00739	9.75
20230	2.64E-05	0.027602	10.25	24743	1.66E-05	0.018903	6.95	88741	2.82E-05	0.011372	8.7
20299	2.89E-05	0.014843	10	24751	2.59E-05	0.001425	5.8	88791	4.27E-05	0.00073	11.75
20316	1.92E-05	0.002159	5.5	24754	4.81E-05	0.006341	10.45	88855	3.83E-05	0.008742	8.95
20399	3.23E-05	0.056556	9.3	24770	1.33E-05	0.015206	5.2	88884	4.24E-05	0.004732	10.5
20404	2.04E-05	0.000778	5.25	24771	2.29E-05	0.023378	8.05	88920	7.83E-05	0.003163	9.75
20406	3.28E-05	0.012147	16.45	24799	1.5E-05	0.011081	5.55	88936	4.94E-05	0.014358	8.8
20411	6.44E-05	0.002236	12.05	24822	1.61E-05	0.011622	6.65	88941	4.21E-05	0.003969	6.7
20469	2.09E-05	0.00102	5.35	24847	1.48E-05	0.006626	6.25	88967	0.000112	0.006598	9.4
								88981	6.91E-05	0.002121	12.45

REPORT DOCUMENTATION PAGE			Form Approved OMB No. 0704-0188	
Public reporting burden for this collection of information is estimated to average 1 hour per response, including the time for reviewing instructions, searching existing data sources, gathering and maintaining the data needed, and completing and reviewing the collection of information. Send comments regarding this burden estimate or any other aspect of this collection of information, including suggestions for reducing this burden, to Washington Headquarters Services, Directorate for Information Operations and Reports, 1215 Jefferson Davis Highway, Suite 1204, Arlington, VA 22202-4302, and to the Office of Management and Budget, Paperwork Reduction Project (0704-0188), Washington, DC 20503.				
1. AGENCY USE ONLY (Leave Blank)	2. REPORT DATE May 2007	3. REPORT TYPE AND DATES COVERED NASA Technical Paper		
4. TITLE AND SUBTITLE ISS Debris Avoidance Maneuver Threshold Analysis			5. FUNDING NUMBERS	
6. AUTHOR(S) M. B. Wortham (United Space Alliance), J.L. Foster (Barrios Technology)				
7. PERFORMING ORGANIZATION NAME(S) AND ADDRESS(ES) Lyndon B. Johnson Space Center Houston, Texas 77058			8. PERFORMING ORGANIZATION REPORT NUMBERS S-1002	
9. SPONSORING/MONITORING AGENCY NAME(S) AND ADDRESS(ES) National Aeronautics and Space Administration Washington, DC 20546-0001			10. SPONSORING/MONITORING AGENCY REPORT NUMBER TP-2007-214752	
11. SUPPLEMENTARY NOTES				
12a. DISTRIBUTION/AVAILABILITY STATEMENT Available from the NASA Center for AeroSpace Information (CASI) 7115 Standard Hanover, MD 21076-1320 Category: 17			12b. DISTRIBUTION CODE	
13. ABSTRACT (Maximum 200 words) The decision for the International Space Station to perform a maneuver to avoid orbital debris will be based upon a predicted collision probability. The collision probability will be calculated using real-time best estimates of the debris and ISS position state and position error covariance, propagated to the anticipated time of conjunction, or time of closest approach (TCA). If the computed collision probability exceeds a threshold value, the Red Threshold, a maneuver will be performed unless prevented by other operational considerations. The debris position and its uncertainty, propagated to TCA, will be supplied by United States Space Command, by processing observations from its Space Surveillance Network. Given the distribution of position errors for a space vehicle and the debris population, it is possible to calculate both the anticipated maneuver rate and the residual risk resulting from the choice of a maneuver threshold. The lower the probability threshold, the more maneuvers will be performed. However, no matter how many maneuvers are performed, risk can never be completely eliminated. Further, the performance of a debris avoidance maneuver disrupts the operation of the ISS micro-gravity laboratory and also complicates altitude management for ISS. Clearly the need is to achieve the maximum possible risk reduction while maintaining a sustainable maneuver rate.				
14. SUBJECT TERMS Space debris, obstacle avoidance, Global Tracking Network, space surveillance, maneuvers			15. NUMBER OF PAGES 48	16. PRICE CODE
17. SECURITY CLASSIFICATION OF REPORT Unclassified	18. SECURITY CLASSIFICATION OF THIS PAGE Unclassified	19. SECURITY CLASSIFICATION OF ABSTRACT Unclassified	20. LIMITATION OF ABSTRACT Unlimited	
